The Journal of Chemical Physics

Electronic couplings for photo-induced processes from subsystem time-dependent density-functional theory: The role of the diabatization

Cite as: J. Chem. Phys. **153**, 184113 (2020); https://doi.org/10.1063/5.0022677
Submitted: 22 July 2020 . Accepted: 27 October 2020 . Published Online: 12 November 2020

Johannes Tölle, Lorenzo Cupellini, Benedetta Mennucci, and Johannes Neugebauer

The Journal of Chemical Physics ARTICLE scitation.org/journal/jcp

Electronic couplings for photo-induced processes from subsystem time-dependent density-functional theory: The role of the diabatization

Cite as: J. Chem. Phys. 153, 184113 (2020); doi: 10.1063/5.0022677
Submitted: 22 July 2020 • Accepted: 27 October 2020 •
Published Online: 12 November 2020

Johannes Tölle,[1] Lorenzo Cupellini,[2] Benedetta Mennucci,[2] and Johannes Neugebauer[1,a)]

AFFILIATIONS

[1]Theoretische Organische Chemie, Organisch-Chemisches Institut and Center for Multiscale Theory and Computation, Westfälische Wilhelms-Universität Münster Corrensstraße 40, 48149 Münster, Germany
[2]Università di Pisa, Dipartimento di Chimica e Chimica Industriale, Via G. Moruzzi 13, 56124 Pisa, Italy

Note: This paper is part of the JCP Special Topic on Excitons: Energetics and Spatio-temporal Dynamics.
[a)]**Author to whom correspondence should be addressed:** j.neugebauer@uni-muenster.de

ABSTRACT

Subsystem time-dependent density-functional theory (sTDDFT) making use of approximate non-additive kinetic energy (NAKE) functionals is known to be capable of describing excitation energy transfer processes in a variety of applications. Here, we show that sTDDFT, especially when combined with projection-based embedding (PbE), can be employed for the entire range of photo-induced electronic couplings essential for modeling photophysical properties of complex chemical and biological systems and therefore represents a complete toolbox for this class of problems. This means that it is capable of capturing the interaction/coupling associated with local- and charge-transfer (CT) excitons. However, this requires the choice of a reasonable diabatic basis. We therefore propose different diabatization strategies of the virtual orbital space in PbE-sTDDFT and show how CT excitations can be included in sTDDFT using NAKE functionals via a phenomenological approach. Finally, these electronic couplings are compared to couplings from a multistate fragment excitation difference (FED)–fragment charge difference (FCD) diabatization procedure. We show that both procedures, multistate FED–FCD and sTDDFT (with the right diabatization procedure chosen), lead to an overall good agreement for the electronic couplings, despite differences in their general diabatization strategy. We conclude that the entire range of photo-induced electronic couplings can be obtained using sTDDFT (with the right diabatization procedure chosen) in a black-box manner.

I. INTRODUCTION

The processes of Excitation Energy Transfer (EET) and Photoinduced Electron Transfer (PET) play a crucial role in the field of material science and biology.[1,2] In photosynthesis, for instance, light is "collected" via the absorption of photons through specifically designed antenna complexes. Subsequently, excitation energy is transferred to a reaction center via EET. In order to convert this energy into chemically accessible energy, charge separation occurs, which is triggered by PET.[3] It becomes obvious that methods that are capable of describing both EET and PET can give insight into design principles used in nature and can help build new artificial photosynthetic systems or to design new solar cells.[4]

These phenomena rely on the interplay of excited states (excitons) located on Donor (D) and Acceptor (A) chromophores and are therefore closely related to the chemical picture of molecular or supermolecular systems consisting of different subsystems. Subsystem-based theoretical approaches, therefore, are obviously appealing to model these phenomena.[5] Especially,

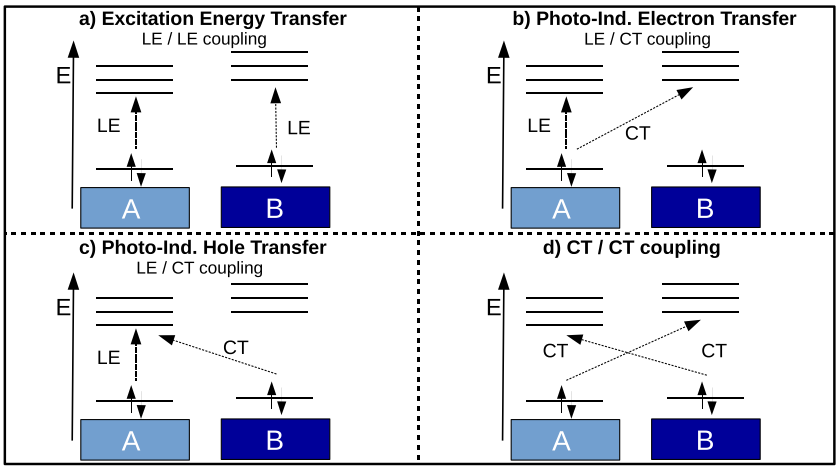

FIG. 1. Different possibilities of the interaction of quasi-diabatic excited states located on different chromophores: (a) The coupling of local excitations (LE) located on A and B, which leads to EET. (b) The coupling of a LE on A and a charge-transfer (CT) excitation from A → B, which leads to an electron transferred from A to B. (c) The coupling of a LE located on A and an incoming CT excitation from B → A, which leads to an hole transferred from A to B. (d) The coupling of two CT excitations from A → B and B → A.

Frozen-Density-Embedding (FDE),[6,7] the related subsystem DFT formalism (sDFT),[8–10] and their extensions to excited states [uncoupled/coupled subsystem Time-Dependent Density Functional Theory (FDEu/FDEc-TDDFT)],[11–13] based on a quantum mechanical (QM) description of the entire system, appear to be well-suited methods in order to model EET and PET phenomena. This raises the question of how to calculate the electronic couplings needed to model such phenomena from these methods. These couplings are directly linked to rate constants in different rate theories, e.g., Förster[14] and Marcus theory.[15] Electronic couplings in the context of EET have already been intensively investigated by means of sTDDFT in combination with approximate non-additive kinetic energy (NAKE) functionals (cf. Refs. 13 and 16–18). By contrast, charge-transfer (CT)/local-excitation (LE) couplings, which are needed to model PET processes, have not been investigated in-depth so far (a first pilot calculation was reported in Ref. 19). This is mostly related to the fact that a description of CT excitations within approximate sTDDFT has not been possible. Recent developments of the so-called exact embedding strategies, relying on projection operators and thus often denoted as projection-based embedding (PbE), for ground-[20] and excited-states,[21] enable the description of CT excitations within sTDDFT.[19] Here and in the following, the term "exact" is used to indicate that supersystem results (of the parent theoretical model without fragmentation) can be exactly restored in the fragment-based description. Exact sTDDFT, in principle, leads to a complete description of electronic couplings involved in EET and PET processes. In Fig. 1, an overview of the possible couplings of excited states located on two subsystems A and B is given. A carefully chosen diabatization strategy is essential in order to extract meaningful electronic couplings for all cases shown in Fig. 1 from the subsystem TDDFT framework as well as from other methods (cf. Refs. 22–25). In the case of sTDDFT, but also for other fragment-based methods, the diabatization procedure is determined by the selection of the fragments. Theoretically, a strictly diabatic basis is obtained if the derivative coupling ($d_{ij} = \langle \Phi_i | \nabla_{\mathbf{R}} | \Phi_j \rangle$) for every nuclear configuration is zero.[26] This requirement is, however, rarely fulfilled and a strict diabatization is often not possible (apart from the conceptual difficulty of calculating such derivate couplings in sDFT). For practical applications, two common definitions of diabatic states exist. The "historical" definition requires the diabatic basis to minimize the derivative coupling. In contrast, the "chemical" definition requires the diabatic basis to maintain the same electronic character along a reaction coordinate,[27,26,28] which is a definition that is easier to control in a sDFT framework. It can be seen that certain ambiguities in the definition of diabatic states exist, which directly translate into differences of the electronic coupling, depending on the diabatization procedures employed. However, not only the diabatization procedure itself but also the physical effects included in the construction of an approximate exciton Hamiltonian can influence the electronic coupling. This influence has been already analyzed in Ref. 29 for solvent screening effects on EET couplings employing a QM/MMpol scheme[30] and approximate sTDDFT. The goal of this paper is therefore twofold. First, we want to establish exact and approximate sTDDFT as a complete toolbox, which is capable of modeling EET and PET processes. Second, we want to compare electronic couplings from sTDDFT to those from other diabatization procedures, which are capable of including LE and CT excitations.

This paper is structured as follows: First, we derive the general theory of sTDDFT without any constraints concerning the embedding method chosen. In a next step, a recently proposed virtual orbital localization in the context of PbE is recaptured. Furthermore, the framework of subsystem TDDFT, employing approximate NAKE functionals, is extended to include CT excitations. Finally, electronic couplings obtained from subsystem TDDFT (PbE, approximate NAKE functionals) are compared to a recently proposed multistate Fragment Excitation Difference (FED)–Fragment Charge Difference (FCD) scheme,[25] which combines the FCD[31] and the FED[32] approach and generalizes it to multiple states.

II. THEORY

A. sDFT

In sDFT,[8–10,6,7] the total electron density of the system is partitioned into electron densities belonging to individual subsystems $\{\rho_I(\mathbf{r})\}$,

$$\rho(\mathbf{r}) = \sum_{I}^{N_s} \rho_I(\mathbf{r}), \tag{1}$$

where the sum runs over all subsystems N_s. Each subsystem is represented by a non-interacting Kohn–Sham- (KS-) like reference system. $\rho_I(\mathbf{r})$ can then obtained from the n_I occupied orbitals $\psi_i(\mathbf{r})$ of subsystem I via

$$\rho_I(\mathbf{r}) = \sum_{i_I}^{n_I} |\psi_i(\mathbf{r})|^2. \tag{2}$$

The total electronic energy E_{el} of the supermolecular system can be expressed in subsystem KS energies E_I^{KS} and the subsystem interaction energies E^{int},

$$E_{\mathrm{el}} = \sum_{I}^{N_s} \underbrace{\{V[\rho_I] + J[\rho_I] + E_{\mathrm{XC}}[\{\rho_I\}] + T_s[\{\psi_{j\sigma}\}_I]\}}_{E_I^{\mathrm{KS}}} + \underbrace{T_s^{\mathrm{nadd}}[\{\rho_I\}] + E_{\mathrm{XC}}^{\mathrm{nadd}}[\{\rho_I\}] + J^{\mathrm{int}}[\{\rho_I\}] + V^{\mathrm{int}}[\{\rho_I\}]}_{E^{\mathrm{int}}}, \tag{3}$$

where $V[\rho_I]$ represents the nucleus–electron interaction, $J[\rho_I]$ represents the electron–electron Coulomb interaction, $E_{\mathrm{XC}}[\{\rho_I\}]$ represents the exchange–correlation energy, and $T_s[\{\psi_j\}_I]$ represents the Kohn–Sham-type kinetic energy of subsystem I. The interaction energy E^{int} contains pair-wise additive $J^{\mathrm{int}}[\{\rho_I\}]$ (Coulomb) and $V^{\mathrm{int}}[\{\rho_I\}]$ (electron–nucleus interaction) contributions and non-additive energy contributions for the kinetic, $T_s^{\mathrm{nadd}}[\{\rho_I\}]$, and exchange–correlation energy, $E_{\mathrm{XC}}^{\mathrm{nadd}}[\{\rho_I\}]$. While the latter can be evaluated consistently with the parent non-subsystem model, using the employed exchange–correlation functional, additional approximations are practically used for the former. The non-additive kinetic energy (NAKE) is defined as

$$T_s^{\mathrm{nadd}}[\{\rho_I\}] = T_s[\rho_{\mathrm{tot}}] - \sum_{I}^{N_s} T_s[\rho_I]. \tag{4}$$

In practice, explicitly density-dependent NAKE functionals are employed for the contribution. Minimization of the energy expression in Eq. (3) under the constraint that the number of electrons in each subsystem stays the same and the densities of the other subsystems are fixed leads to the so-called Kohn–Sham equations with Constrained Electron Density (KSCED),[7]

$$\left(-\frac{\nabla_i^2}{2} + v_s[\{\rho_I\}](\mathbf{r}) + v_{\mathrm{emb}}^I[\{\rho_I\},\rho](\mathbf{r})\right)\psi_i^I(\mathbf{r}) = \epsilon_i^I \psi_i^I(\mathbf{r}), \tag{5}$$

where the interaction with the environment is expressed through $v_{\mathrm{emb}}^I[\{\rho_I\},\rho](\mathbf{r})$, which is defined as

$$\begin{aligned} v_{\mathrm{emb}}^I[\{\rho_I\},\rho] &= \sum_{K\neq I}\left[\int \frac{\rho_K(\mathbf{r})}{|\mathbf{r}-\mathbf{r}'|}d\mathbf{r}' - \sum_{\alpha\in K}\frac{Z_\alpha}{|\mathbf{r}-\mathbf{R}_\alpha|}\right] + \frac{\delta T_s[\rho_{\mathrm{tot}}]}{\delta\rho_{\mathrm{tot}}(\mathbf{r})} \\ &\quad - \frac{\delta T_s[\rho_{I\sigma}]}{\delta\rho_I(\mathbf{r})} + \frac{\delta E_{\mathrm{XC}}[\rho_{\mathrm{tot}}]}{\delta\rho_{\mathrm{tot}}(\mathbf{r})} - \frac{\delta E_{\mathrm{XC}}[\rho_I]}{\delta\rho_{I\sigma}(\mathbf{r})} \\ &= \sum_{K\neq I}\left[v_{\mathrm{coul}}[\rho_K](\mathbf{r}) + v_{\mathrm{nuc}}^K(\mathbf{r})\right] + v_{\mathrm{nadd}}[\rho_{\mathrm{tot}},\rho_I](\mathbf{r}). \end{aligned} \tag{6}$$

In Eq. (6), the electron–electron Coulomb interaction with the environment subsystems is denoted as $v_{\mathrm{coul}}[\rho_K](\mathbf{r})$, the interaction with the nuclei in the environment is denoted as $v_{\mathrm{nuc}}^K(\mathbf{r})$, and the non-additive kinetic energy and exchange–correlation potential are summarized in $v_{\mathrm{nadd}}[\rho_{\mathrm{tot}}, \rho_I](\mathbf{r})$. For further details concerning subsystem DFT using approximate NAKE functionals, see Refs. 33–38.

1. Projection-based embedding

The fragmentation approach introduced in Sec. II A is conceptually and computationally very appealing. However, practical realizations are limited by the available NAKE functional approximations. A workaround to this problem has been proposed by Manby *et al.*,[20] which will be called projection-based embedding (PbE) in the following. In this embedding approach, a projection operator is used instead of the NAKE functional, and consequently, the subsystem kinetic energies are additive. This ensures orthogonality between orbitals of different subsystems. Within this approach, supermolecular KS-DFT results can be restored, assuming that a supermolecular basis and the same functionals are used for the individual subsystems and their interactions.[20,39] As already shown and numerically demonstrated in Ref. 19, PbE (with supermolecular basis and the same functionals for each subsystem) leads to a virtual orbital space, which is identical for all subsystems due to the non-local nature of the projection operator employed. This further implies that the orbital-transition space for each subsystem also contains CT orbital transitions from one subsystem to another (outgoing CT transitions).[19] Note that this cannot be achieved via the usage of local NAKE functionals.[40]

B. sTDDFT

In sTDDFT, the full density response $\delta\rho(\mathbf{r})$ is partitioned into density response functions belonging to individual subsystems $\delta\rho_I(\mathbf{r})$,

$$\delta\rho(\mathbf{r},\omega) = \sum_I \delta\rho_I(\mathbf{r},\omega). \tag{7}$$

The density response of subsystem I determined through a frequency (ω) dependent perturbation $\delta v_I(\mathbf{r}', \omega)$ is given as

$$\delta\rho_I(\mathbf{r},\omega) = \int \chi_s^I(\mathbf{r},\mathbf{r}',\omega)\delta v^I(\mathbf{r}',\omega)d\mathbf{r}, \tag{8}$$

where the noninteracting Kohn–Sham response function of subsystem I is denoted as $\chi_s^I(\mathbf{r},\mathbf{r}',\omega)$. Following the derivation of sTDDFT in Refs. 41 and 19 leads to the following non-Hermitian eigenvalue problem:

$$\begin{pmatrix}\mathbf{A} & \mathbf{B}\\ \mathbf{B} & \mathbf{A}\end{pmatrix}\begin{pmatrix}\mathbf{X}\\ \mathbf{Y}\end{pmatrix} = \omega\begin{pmatrix}-\mathbf{1} & \mathbf{0}\\ \mathbf{0} & \mathbf{1}\end{pmatrix}\begin{pmatrix}\mathbf{X}\\ \mathbf{Y}\end{pmatrix}, \tag{9}$$

where the response matrices $\mathbf{A}$ and $\mathbf{B}$ are given in terms of occupied-virtual subsystem orbital transitions. The individual matrix elements are given as

$$A_{(ia)_I,(jb)_J} = \delta_{IJ}\delta_{ij}\delta_{ab}(\epsilon_a^I - \epsilon_i^I) + K_{(ia)_I,(jb)_J} \tag{10}$$

and

$$B_{(ia)_I,(jb)_J} = K_{(ia)_I,(bj)_J}. \tag{11}$$

For the response matrices, the usual notation for occupied i, j, ... and virtual orbitals a, b, ... is employed. In Eqs. (10) and (11), the intrinsic subsystem structure is indicated via (capital indices) I, J, ..., orbital energies are given as ϵ, and the so-called coupling matrix elements $K_{(ia)_I,(jb)_J}$ are, in general, defined as

$$\begin{aligned} K_{(ia)_I,(jb)_J} = &\left(i^I a^I \mid j^J b^J\right) + \left(i^I a^I \mid f_{\mathrm{xc}}(\mathbf{r},\mathbf{r}') \mid j^J b^J\right) - c_{\mathrm{x}}\left(i^I j^J \mid a^I b^J\right) \\ &+ \left(i^I a^I \mid f_{\mathrm{kin}}(\mathbf{r},\mathbf{r}') \mid j^J b^J\right) - \delta_{IJ}\left(i^I a^I \mid f^I_{\mathrm{kin}}(\mathbf{r},\mathbf{r}') \mid j^J b^J\right) \\ &+ (1-\delta_{IJ})\, \hat{O}^{\mathrm{EO}}_{(ia)_I,(bj)_J}. \end{aligned} \tag{12}$$

Here, the Mulliken notation is employed. The kinetic (f_{kin}) and exchange–correlation (f_{xc}) kernel contributions are obtained by taking the derivative of the electronic potential of subsystem I with respect to the electron density ρ_J.[13] Note that Eq. (12) is given in a general form of the coupling matrix used in sTDDFT and contains all possible coupling matrix contributions. While Coulomb and exchange–correlation contributions (first and second term) are taken into account in sTDDFT independently of the ground-state embedding procedure employed, the exact exchange (third term) in this form is only strictly applicable for orthogonal orbitals. Furthermore, the approximate NAKE kernel contribution (fourth term) occurs only if approximate NAKE functionals are employed in the ground-state embedding procedure.[11,13] In contrast to that, the external-orthogonality (EO) contribution $\hat{O}^{\mathrm{EO}}_{(ia)_I,(bj)_J}$ occurs only in PbE calculations. A detailed derivation for this contribution in the context of different projection operators can be found in Ref. 19.

In Ref. 13, the first practical realization of the sTDDFT eigenvalue problem was proposed. There, the response problem is solved in two steps. First, the so-called uncoupled (denoted as FDEu-TDDFT in the following), excitation energies and vectors are obtained by taking only intra-subsystem orbital transitions into account. This means that only the response of a particular subsystem is taken into account, while additional environment contributions and excited-state polarization effects of the environment due to an excitation are omitted. It is obvious that this step is trivially parallelizable for a large number of subsystems at the same time. In a next step, the individual FDEu-TDDFT excitation vectors are used to transform the response problem in Eq. (9) into the space spanned by the FDEu-TDDFT excitation vectors (for a detailed information about this procedure, see Ref. 13 for a Hermitian formulation of the sTDDFT response problem and Ref. 19 for a non-Hermitian formulation). Note that this procedure is only exact if a full uncoupled excitation space[21] is employed. In practice, however, the transformation is often approximated by including only a small subset of uncoupled excitation vectors in the transformation. The usage of the Hermitian formulation of the response problem in the context of PbE is only an approximation, and the non-Hermitian response problem should be solved instead.[21]

C. Diabatization and orbital space selection within sTDDFT

In Sec. II B, the linear-response TDDFT equations within a subsystem-based framework are derived. There, no particular comment concerning the orbital-transition space of a certain subsystem I was made. In most of the applications of sTDDFT, the orbital-transition space is determined by the basis set used for a particular subsystem. If a monomer basis is employed, only local orbital-transitions and therefore only local excitations are obtained. If a supermolecular basis set is employed, both LE and CT excitations can, in principle, be obtained. While PbE FDEu/FDEc-sTDDFT calculations have been proven to correctly describe CT excitations (within the accuracy of the exchange–correlation functional chosen), approximate FDEu/c-sTDDFT fails to correctly describe CT excitations.[19] Note that this holds also true for the exact NAKE functional, as already observed by Jacob *et al.*[40]

The goal of this work is the calculation of electronic couplings involved in EET and PET phenomena by means of sTDDFT and PbE, but we will also assess if this calculation is possible with approximate NAKE functionals. To this end, it is necessary to correctly describe the diabatic LE and CT states in the preliminary FDEu-TDDFT step in order to extract meaningful electronic couplings from the subsequent FDEc-TDDFT calculations. We therefore introduce three different diabatization procedures acting on the virtual orbitals in order to define LE and CT orbital transition subspaces.

Within PbE-sTDDFT (using a supermolecular basis set; taking all atomic orbitals of the entire system for the linear combination of the molecular orbitals of each subsystem into account), the LE and CT excitations are naturally included because the virtual orbital space of each subsystem contains the supermolecular canonical virtual orbital space.[19] A trivial separation scheme for LE and CT excitations is possible, as proposed in Ref. 19. There, the virtual supermolecular canonical orbital space was partitioned based on a modified overlap criterion,

$$S^I_{aa} = \sum_{\nu\in I}\sum_{\mu\in I,J} C^I_{\nu a} C^I_{\mu a} S_{\nu\mu}, \tag{13}$$

where the sums run over the basis function of subsystem I and the combined basis functions of I and J, respectively. The orbitals are assigned to be located on subsystem I based on the value of the modified overlap, which quantifies how much of the orbital can be represented by the basis functions of subsystem I. Note that this idea represents a selection of virtual orbitals rather than a strict diabatization and will therefore be denoted as canonical partitioning in the following.

A more sophisticated LE/CT separation can be obtained via our recently proposed virtual-orbital localization procedure.[42] This procedure can be employed to obtain virtual orbitals located on the particular subsystem or on the environment. This intrinsically restricts the orbital-transition space in the uncoupled calculation to be either purely local or CT. The localization procedure is based on the SPADE algorithm proposed for occupied orbitals in the context of PbE[43] and will be briefly repeated here. First, the virtual orbital block of the coefficient matrix is orthogonalized,

$$\tilde{\mathbf{C}}_{\mathrm{virt}} = \mathbf{S}^{\frac{1}{2}}\mathbf{C}_{\mathrm{virt}}. \tag{14}$$

Then, the MO overlap matrix is constructed from the AO basis of subsystem A,

$$S^{\mathrm{A}}_{a,b} = \sum_{v\in A} \tilde{C}_{v,a}\tilde{C}_{v,b}. \tag{15}$$

Performing a Singular Value Decomposition (SVD) of $\mathbf{S}^{\mathrm{A}}$,

$$\mathbf{S}^{\mathrm{A}} = \mathbf{U}^{\mathrm{A}}\mathbf{\Sigma}^{\mathrm{A}}\mathbf{V}^{\mathrm{A}}, \tag{16}$$

the localized virtual orbitals can be obtained as

$$\tilde{\mathbf{C}}_{\mathrm{virt}} = \mathbf{C}_{\mathrm{virt}}\mathbf{V}^{\mathrm{A}}. \tag{17}$$

Based on the singular value of a given orbital (between 0 and 1), the orbital is assigned to be located on the particular subsystem (>0.5) or on the environment subsystem (<0.5). In a next step, it is ensured that the chosen virtual orbitals diagonalize the embedded Fock-matrix $\mathbb{F}^{\mathrm{A}}$ of subsystem A. For this, the Fock matrix is transformed into the space spanned by the chosen virtual coefficients and diagonalized,

$$\mathbb{F}^{\mathrm{A}} = \tilde{\mathbf{C}}^{\mathrm{A},T}_{\mathrm{virt}}\mathbf{F}^{\mathrm{A(Env)}}\tilde{\mathbf{C}}^{\mathrm{A}}_{\mathrm{virt}}, \tag{18}$$

$$\lambda = \mathbb{C}^{\mathrm{A},T}_{\mathrm{virt}}\mathbb{F}^{\mathrm{A}}\mathbb{C}^{\mathrm{A}}_{\mathrm{virt}}, \tag{19}$$

where λ contains the new orbital energies associated with the localized virtual orbitals. The new virtual orbital coefficients can then obtained as

$$\mathbf{C}^{\mathrm{A}}_{\mathrm{virt}} = \tilde{\mathbf{C}}_{\mathrm{virt}}\mathbb{C}^{\mathrm{A}}. \tag{20}$$

Choosing the sets of occupied and virtual orbitals belonging to a particular subsystem defines the orbital-transition space in the FDEu-TDDFT calculations (local or CT).

However, due to this additional virtual orbital localization step, an additional set of coupling matrix contributions needs to be taken into account. In Ref. 19, an analysis of the external-orthogonality coupling matrix contributions revealed that these contributions arise from off-diagonal Lagrange multipliers. In the case of the Huzinaga projection operator, these have the following form:

$$\hat{O}^{\mathrm{EO}}_{(ia)_I,(jb)_J} = -F^{IJ}_{ij}S^{IJ}_{ab}, \tag{21}$$

where F^{IJ}_{ij} denotes the occupied–occupied off-diagonal block of the Fock matrix and S^{IJ}_{ab} is the virtual–virtual orbital overlap between subsystem I and J. Due to the fact that the orbitals of two subsystems in PbE are exactly orthogonal if a supermolecular basis set is employed, S^{IJ}_{ab} can be rewritten as δ^{IJ}_{ab}. If an additional virtual orbital localization procedure is performed, a new set of coupling matrix contributions need to be taken into account corresponding to the virtual–virtual off-diagonal block of the Fock matrix F^{IJ}_{ab} between subsystems I and J. The final contributions to the coupling matrix due to the usage of localized molecular orbitals are then given as

$$\hat{O}^{\mathrm{EO}}_{(ia)_I,(jb)_J} = \underbrace{F^{IJ}_{ab}\delta^{IJ}_{ij}}_{\hat{O}^{\mathrm{EO,virt}}_{(ia)_I,(jb)_J}} - \underbrace{F^{IJ}_{ij}\delta^{IJ}_{ab}}_{\hat{O}^{\mathrm{EO,occ}}_{(ia)_I,(jb)_J}}. \tag{22}$$

In the special case that the inter-subsystem Fock matrix blocks for occupied and virtual orbitals are zero (diagonal Fock matrix), $\hat{O}^{\mathrm{EO}}_{(ia)_I,(jb)_J}$ is zero and only orbital energy differences as described in Eq. (10) will enter the response equations.

In contrast to PbE sTDDFT, in approximate sTDDFT, a monomer basis set is used, which includes only basis functions associated with atoms of a particular subsystem, and the orbital transition space is intrinsically enforced to be local, leading to LE only. A description of CT states has not been possible so far in that context. Nevertheless, methods have been developed to describe CT excitations within the approximate sDFT formalism.[44–47] Here, a practically motivated approach to incorporate CT orbital-transitions in the approximate sTDDFT framework is chosen. In this approach, a regular ground-state sDFT calculation employing an approximate NAKE functional and a monomer basis is performed. For CT states, the occupied orbitals of one subsystem are combined with the virtual orbitals located on an environment subsystem, and the basis set is extended with the basis functions located on the environment subsystem. The newly obtained orbital space consists of occupied orbitals on one subsystem and virtual orbitals located on an environment subsystem, which leads to the appearance of CT excitations in the FDEu-TDDFT calculation.

As the combined orbital space is not necessarily orthogonal,[48] we use a procedure that corrects for the non-orthogonality. In a first step, we set up a projector that removes occupied contributions from the newly chosen virtual orbitals,

$$|\tilde{\psi}_a\rangle = \left(1 - \sum_{i\in A}|\psi_i\rangle\langle\psi_i|\right)|\psi_a\rangle. \tag{23}$$

The new set of transformed virtual orbitals $\{\tilde{\psi}_a\}$ can, in principle, contain linear dependencies. These need to be removed, and the orbitals need to be renormalized. The final orbitals and orbital energies are obtained via diagonalization of the subsystem Fock matrix transformed into the space of the projected virtual orbitals $\{\tilde{\psi}_a\}$ [similar to Eqs. (18) and (19)].

D. Electronic couplings from sTDA

In this subsection, the general procedure for the evaluation of electronic couplings from the subsystem Tamm–Dancoff-Approximation (sTDA) is described.[17] The aim is to illustrate the procedure used in Sec. IV for the extraction of electron couplings from sTDA. Note that, in principle, the extraction of electronic couplings from the sTDDFT formulation of Ref. 13 is also possible. This has been accomplished via the diagonalization of CI-like 2 × 2 eigenvalue problems,[16] which, however, is an approximation. We illustrate the procedure using two example subsystems A and B. Nevertheless, a generalization to an arbitrary number of subsystems is possible.

The workflow is illustrated in Fig. 2. In a first step [Fig. 2 (a)], one of the diabatization procedures proposed in Sec. II C is used to separate the virtual orbital spaces from a ground-state embedding calculation into local and charge transfer. In this way, each orbital transition $i \rightarrow a$ can be classified as local (if a is located on the same subsystem as i) or charge transfer (if a is located on an environment subsystem). In a next step, FDEu-TDA calculations for the subsystems and their local and charge-transfer orbital-transitions spaces

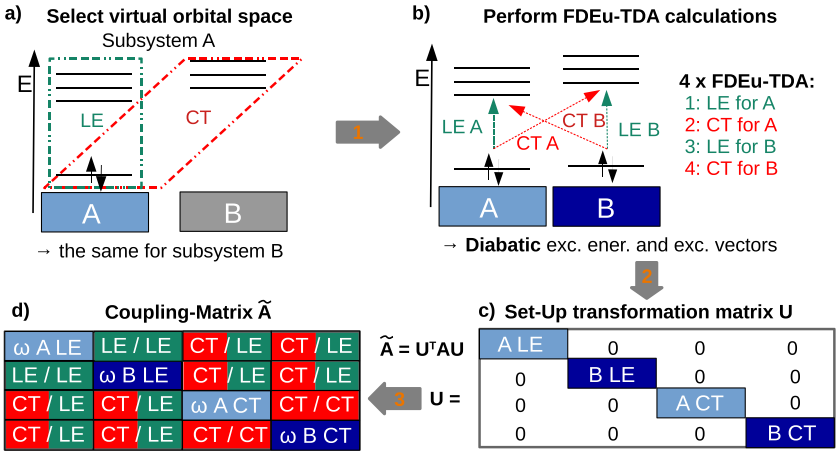

FIG. 2. Schematic illustration of the coupling procedure: (a) selection of the virtual orbital space, (b) calculation of FDEu-TDA excitation energies and eigenvectors within the chosen orbital-transition space, (c) setup of the transformation matrix for the coupling procedure consisting of uncoupled eigenvectors belonging to a certain orbital-transition space on the block-diagonal, and (d) response matrix transformation and determination of electronic couplings.

are performed, respectively. In the case of two subsystems, this corresponds to a total of four FDEu-TDA calculations (A: LE, A: CT, B: LE, and B: CT) [Fig. 2(b)]. The resulting excitation energies are the diabatic excitation energies associated with the orbital-transition space of a particular subsystem.

Then, the transformation matrix is set up from the uncoupled excitation vectors. The matrix **U** [Fig. 2(c)] is block-diagonal, and each block contains the uncoupled excitation vectors associated with the uncoupled excitations determined in the FDEu-TDA calculations. For the two subsystems, the transformation matrix contains four blocks associated with the subsystem and the particular orbital-transition space [Fig. 2(c)]. This transformation matrix **U** is then used to transform the matrix **A** [Eq. (10)], which contains all occupied-virtual orbital transitions of the individual subsystems $\tilde{\mathbf{A}} = \mathbf{U}^T\mathbf{A}\mathbf{U}$. This step is denoted as the "coupling" step or FDEc-TDA because the responses of the individual subsystems are coupled. The off-diagonal blocks of matrix $\tilde{\mathbf{A}}$ correspond to the couplings between excited states previously calculated in the FDEu-TDA calculations and the diagonal contain the diabatic FDEu-TDA excitation energies [Fig. 2(d)]. An overview of the different coupling matrix contributions taken into account in FDEu- and FDEc-TDA calculations for PbE and approximate NAKE functionals is shown in Table I. Diagonalizing $\tilde{\mathbf{A}}$ gives access to coupled adiabatic excitation energies and excitation vectors. In the case of PbE with an additional virtual orbital space localization procedure, the exact supermolecular excitation energies are obtained if the complete uncoupled subspace is used for the transformation to $\tilde{\mathbf{A}}$.

E. Multistate FED–FCD

An alternative approach for the determination of electronic couplings as shown in Fig. 1 is achieved via the automated multistate Fragment Charge Difference (FCD)–Fragment Excitation Difference (FED) approach.[25] It combines the FCD scheme proposed by Voityuk and Rösch[31] and the FED scheme developed by Hsu *et al.*[49] and can be seen as an extension to the multistate-FCD scheme proposed by Hsu and co-workers in 2013.[32] In the following, the fundamentals of this approach are recaptured.

All these approaches have in common that they partition the total system into two fragments/subsystems A/B. In order to extract electronic couplings, both approaches (FCD and FED) set up a transformation matrix from the adiabatic to the diabatic basis, which is located on A and B, respectively. In the case of the FED scheme, this transformation can be obtained via the excitation difference matrix $\Delta\mathbf{x}$. The entries are defined as

$$\Delta x_{nm} = \int_{r\in B} \rho^{ex}_{nm}(\mathbf{r})d\mathbf{r} - \int_{r\in A} \rho^{ex}_{nm}(\mathbf{r})d\mathbf{r}, \tag{24}$$

where the excitation density is obtained from the sum of the electron and hole densities. In the case of CIS/TDA, the excitation density is defined as[50]

$$\rho^{ex}_{nm}(\mathbf{r}) = \sum_{ij}\sum_{a} t^{m}_{ia}t^{n*}_{ja}\phi_i(\mathbf{r})\phi^*_j(\mathbf{r}) + \sum_{i}\sum_{ab} t^{m}_{ia}t^{n*}_{ib}\phi_a(\mathbf{r})\phi^*_b(\mathbf{r}). \tag{25}$$

The CIS/TDA coefficients of states m/n are given as t^m_{ia} and t^n_{ia}, respectively. From Eq. (25), it can be seen that fragment excitation differences between −2 and 2 are obtained. These correspond to completely localized excitations either on *A* or *B* and the eigenvectors of Δx_{nm} can be used to transform the adiabatic excitation energies to a localized diabatic basis and to extract the corresponding electronic couplings as we will see later.

A similar approach is used in the FCD method, where a charge difference matrix $\Delta\mathbf{q}$ is used for the diabatization procedure. The elements of the charge difference matrix Δq_{nm} are defined as

$$\Delta q_{nm} = \int_{r\in D} \rho_{nm}(\mathbf{r})d\mathbf{r} - \int_{r\in A} \rho_{nm}(\mathbf{r})d\mathbf{r}, \tag{26}$$

where $\rho_{nm}(\mathbf{r})$ represents the transition density between state *n* and *m*. In the case of $n = m$, it resembles the state density. Δq_{nm} has extrema between 2 and −2 for charge transfer states ($A^+ \cdot B^-$) and vice versa.

The multistate FED–FCD[25] approach makes use of the FCD and FED methods to separate LE/CT subspaces for multiple states. In order to be consistent with Ref. 25, the two matrices $\Delta\mathbf{q}$ and $\Delta\mathbf{x}$ are multiplied with factors of $\frac{1}{2}$, which leads to extrema between −1

TABLE I. Coupling matrix contributions taken into account in FDEu- and FDEc-TDA calculations for projection-based embedding (PbE) (canon. refers to the canonical partitioning of the virtual orbital space, as described in Sec. II C and loc. refers to the virtual orbital localization procedure, as described in Sec. II C) and embedding making use of approximate NAKE functionals. Mulliken notation is used throughout. The individual coupling matrix contributions are introduced in Eqs. (12) and (22).

FDEu of A			
Coupling matrix contribution $K_{(ia)_A,(jb)_A}$	PbE canon.	PbE loc.	approx. NAKE
$(i^A a^A \vert j^A b^A)$ Eq. (12)	✓	✓	✓
$\left(i^A a^A \mid f_{\mathrm{xc}}(\mathbf{r},\mathbf{r}') \mid j^A b^A\right)$	✓	✓	✓
$\left(i^A j^A \mid a^A b^A\right)$	✓	✓	✓
$\left(i^A a^A \mid f_{\mathrm{kin}}(\mathbf{r},\mathbf{r}') \mid j^A b^A\right) - \left(i^A a^A \mid f^A_{\mathrm{kin}}(\mathbf{r},\mathbf{r}') \mid j^A b^A\right)$	X	X	✓
FDEc of A and B			
Coupling matrix contribution $K_{(ia)_A,(jb)_B}$	PbE canon.	PbE loc.	approx. NAKE
$(i^A a^A \vert j^B b^B)$	✓	✓	✓
$\left(i^A a^A \mid f_{\mathrm{xc}}(\mathbf{r},\mathbf{r}') \mid j^B b^B\right)$	✓	✓	✓
$\left(i^A j^B \mid a^A b^B\right)$	✓	✓	X
$\left(i^A a^A \mid f_{\mathrm{kin}}(\mathbf{r},\mathbf{r}') \mid j^B b^B\right)$	X	X	✓
$\hat{O}^{\mathrm{EO,occ}}_{(ia)_A,(jb)_B} = -F^{IJ}_{ij}\delta^{IJ}_{ab}$	✓	✓	X
$\hat{O}^{\mathrm{EO,virt}}_{(ia)_A,(jb)_B} = F^{IJ}_{ab}\delta^{IJ}_{ij}$	X	✓	X

and 1. In a first step, the LE/CT subspaces are separated via a newly defined matrix **D**,

$$\mathbf{D} = (\Delta\mathbf{q})^2 - (\Delta\mathbf{x})^2. \tag{27}$$

The diagonalization of **D** leads to eigenvalues between 1 and −1 corresponding to the LE and CT subspaces, respectively,

$$\mathbf{U}_1^T \mathbf{D} \mathbf{U}_1 = \mathbf{D}'. \tag{28}$$

$\Delta\mathbf{q}$ and $\Delta\mathbf{x}$ are then transformed in the space spanned by $\mathbf{U}_1$ to obtain $\Delta\mathbf{q}'$ and $\Delta\mathbf{x}'$. Based on the eigenvalues of $\mathbf{D}'$, the states are assigned to be LE or CT. The corresponding blocks in $\Delta\mathbf{q}'$ and $\Delta\mathbf{x}'$ are then diagonalized,

$$\mathbf{U}^T_{2(\mathrm{CT})} \Delta\mathbf{q}'_{\mathrm{CT}} \mathbf{U}_{2(\mathrm{CT})} = \Delta\mathbf{q}'', \tag{29}$$

$$\mathbf{U}^T_{2(\mathrm{LE})} \Delta\mathbf{x}'_{\mathrm{LE}} \mathbf{U}_{2(\mathrm{LE})} = \Delta\mathbf{x}''. \tag{30}$$

From this, the second transformation matrix $\mathbf{U}_2$ can be constructed. $\mathbf{U}_2$ contains $\mathbf{U}_{2(\mathrm{CT})}$ and $\mathbf{U}_{2(\mathrm{LE})}$ on the diagonal and rotates the LE and CT subspaces separately,

$$\mathbf{U}_2 = \begin{pmatrix} \mathbf{U}_{2(\mathrm{CT})} & 0 \\ 0 & \mathbf{U}_{2(\mathrm{LE})} \end{pmatrix}. \tag{31}$$

The adiabatic excitation energies can then be transformed to the diabatic basis via $\mathbf{U}_2^T\mathbf{U}_1^T\mathbf{E}\mathbf{U}_1\mathbf{U}_2 = \mathbf{H}''$, where **E** contains the adiabatic excitation energies on the diagonal. The values of $\Delta\mathbf{q}''$ and $\Delta\mathbf{x}''$ in the CT and LE subspaces can then be used to divide the individual CT (CT1: A^+B^- and CT2: A^-B^+) and LE (LE1: A^*B and LE2: B^*A) subspaces even further. The Hamiltonian within each subspace is required to be diagonal. Therefore, in a last step, a block diagonal transformation matrix $\mathbf{U}_3$ is set up, which diagonalizes the four subspaces separately,

$$\begin{aligned} \mathbf{U}_3^T \begin{pmatrix} \mathbf{H}''_{\mathrm{CT1}} & \mathbf{H}''_{\mathrm{CT1,CT2}} & \mathbf{H}''_{\mathrm{CT1,LE1}} & \mathbf{H}''_{\mathrm{CT1,LE2}} \\ \mathbf{H}''_{\mathrm{CT2,CT1}} & \mathbf{H}''_{\mathrm{CT2}} & \mathbf{H}''_{\mathrm{CT2,LE1}} & \mathbf{H}''_{\mathrm{CT2,LE2}} \\ \mathbf{H}''_{\mathrm{LE1,CT1}} & \mathbf{H}''_{\mathrm{LE1,CT2}} & \mathbf{H}''_{\mathrm{LE1}} & \mathbf{H}''_{\mathrm{LE1,LE2}} \\ \mathbf{H}''_{\mathrm{LE2,CT1}} & \mathbf{H}''_{\mathrm{LE2,CT2}} & \mathbf{H}''_{\mathrm{LE2,CT1}} & \mathbf{H}''_{\mathrm{LE2}} \end{pmatrix} \mathbf{U}_3 \\ = \begin{pmatrix} \epsilon'''_{\mathrm{CT1}} & \mathbf{H}'''_{\mathrm{CT1,CT2}} & \mathbf{H}'''_{\mathrm{CT1,LE1}} & \mathbf{H}'''_{\mathrm{CT1,LE2}} \\ \mathbf{H}'''_{\mathrm{CT2,CT1}} & \epsilon'''_{\mathrm{CT2}} & \mathbf{H}'''_{\mathrm{CT2,LE1}} & \mathbf{H}'''_{\mathrm{CT2,LE2}} \\ \mathbf{H}'''_{\mathrm{LE1,CT1}} & \mathbf{H}'''_{\mathrm{LE1,CT2}} & \epsilon'''_{\mathrm{LE1}} & \mathbf{H}'''_{\mathrm{LE1,LE2}} \\ \mathbf{H}'''_{\mathrm{LE2,CT1}} & \mathbf{H}'''_{\mathrm{LE2,CT2}} & \mathbf{H}'''_{\mathrm{LE2,CT1}} & \epsilon'''_{\mathrm{LE2}} \end{pmatrix}. \end{aligned} \tag{32}$$

III. COMPUTATIONAL DETAILS

All calculations were performed with a development version of SERENITY.[51,52] If not stated otherwise, the notation of the functional combination in the subsystem calculation is given as exchange–correlation functional (XCFunc)/non-additive XCFunc/NAKE or projection operator. In the case of TDDFT calculations, the respective kernel contributions within the adiabatic approximation are evaluated with the same functionals as the ground-state potentials. Monomer basis sets are used throughout this

study in approximate sDFT calculations, and supersystem basis sets are employed in projection-based embedding (PbE) sDFT calculations.

For embedding calculations making use of approximate NAKE functionals, the subsystem densities were relaxed through a Freeze-and-Thaw (FaT) procedure until the sum of the absolute change in all density matrix entries was below 10^{-5}. For PbE sDFT calculations, a top-down embedding procedure[39] is used, where orbitals of each subsystem are relaxed.[42,53] Further details concerning functionals and/or projection operators used in the calculations are given in each subsection individually.

In Sec. II C, three diabatization approaches in the context of sDFT have been proposed. These procedures are referred to as (i) "canonical" when the canonical virtual orbital space of a projection-based embedding calculation is partitioned, (ii) as "localization" when the virtual orbital space of a projection-based embedding calculation is additionally localized on the subsystem or on the environment subsystem, or (iii) as "approximate" when the occupied and virtual orbital spaces of different subsystems from a sDFT calculation with an approximate NAKE functional are combined. For the approximate diabatization scheme, an additional orbital orthogonalization step [as described in Eq. (23)] is denoted as "relaxation." The general procedure for the calculation of electronic couplings and diabatic excitation energies in sTDDFT then proceeds, as described in Sec. II D and depicted in Fig. 2. In the case of PbE calculations, artificially shifted occupied environment orbitals are removed from the virtual orbital space of the active subsystem for sTDDFT calculations.[19]

The multistate FED–FCD diabatization procedure[25] has been implemented in Serenity, and the matrices $\Delta\mathbf{q}$ and $\Delta\mathbf{x}$ are constructed using Löwdin charges in contrast to the Mulliken charges used in Ref. 49. All multistate FED–FCD calculations have been performed with supermolecular adiabatic TDA excitation energies and vectors.

All calculations were performed employing the Resolution of the Identity (RI) approximation[54] for the evaluation of the Coulomb contribution in DFT and TDDFT[55] calculations.

IV. RESULTS AND DISCUSSION

A. Ethylene–tetrafluroethylene

In order to compare and test LE/LE and LE/CT electronic couplings from different sTDA diabatization strategies (Sec. II C) but also with respect to other diabatization procedures often employed in the literature,[31,49,32,25] the ethylene–tetrafluoroethylene dimer is chosen as a benchmark system. The structure was taken from Ref. 19 and arranged, as shown in Fig. 3 for varying displacements between 4 Å and 6 Å.

The CAMB3LYP[56] exchange–correlation functional contribution is used throughout for the intra-subsystem exchange correlation. The CAMB3LYP and BLYP[57,58] functionals are employed for the non-additive exchange–correlation contributions, while the LLP91[59] NAKE functional (for approximate sDFT/sTDDFT) or the "Levelshift" projection operator[20] (for PbE-sTDA/sTDDFT) has been applied in combination with the def2-SVP and the def2-TZVP basis set.[60] In summary, this means that for sTDA employing PbE (denoted as sTDA-PbE), the CAMB3LYP/CAMB3LYP/Levelshift functional combination is chosen. For calculations employing approximate NAKE functionals (denoted as sTDA-NAKE), the CAMB3LYP/BLYP/LLP91 functional combination is used. Multistate FED–FCD calculations were performed using 20 states from a supermolecular TDA calculation.

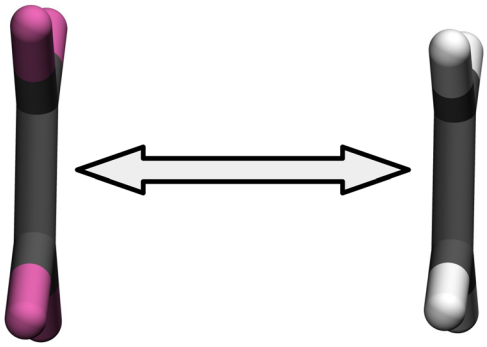

FIG. 3. Ethylene–tetrafluoroethylene dimer as taken from Ref. 19. The displacement between the two monomers is illustrated via a black arrow.

1. Diabatic CT excitations

In a first step, we want to compare the diabatic excitation energies of the $\pi \rightarrow \pi^*$ CT transition from tetrafluoroethylene to ethylene for varying inter-subsystem displacements. The three diabatization procedures proposed in Sec. II C for sTDDFT/sTDA are compared among themselves but also with respect to the multistate FED–FCD scheme.[25] The corresponding excitation energies for the def2-SVP (a) and def2-TZVP (b) basis set are displayed in Fig. 4. Furthermore, the Highest Occupied Molecular Orbital (HOMO) and Lowest Unoccupied Molecular Orbital (LUMO) for PbE with and without the virtual orbital localization procedure for the def2-SVP basis set are shown in Fig. 5, which illustrates the difference between the two diabatization procedures for this example.

As expected,[61] CT excitation energies increase with increasing inter-subsystem displacement. Furthermore, all methods converge to the same excitation energy for larger subsystem displacements for both basis sets. However, the convergence for the different methods is faster for the smaller def2-SVP basis set. This convergence behavior is expected and is caused by a decrease in the differential orbital overlap between orbitals located on the two subsystems with an increase in the inter-subsystem displacement. It represents an important sanity check for the different methods.

By comparison of the excitation energies obtained for the def2-SVP basis set [Fig. 4(a)], only small deviations among the subsystem-based methods can be observed. Interestingly, excitation energies from the approximate FDEu-TDA method are almost identical to the PbE localized virtual orbital FDEu-TDA approach (denoted as "localization" in Fig. 4). By contrast, excitation energies obtained with the canonical virtual orbital space partitioning scheme (denoted as "canonical" in Fig. 4) are slightly shifted to higher energy for subsystem separations from 4.2 Å to 5.4 Å.

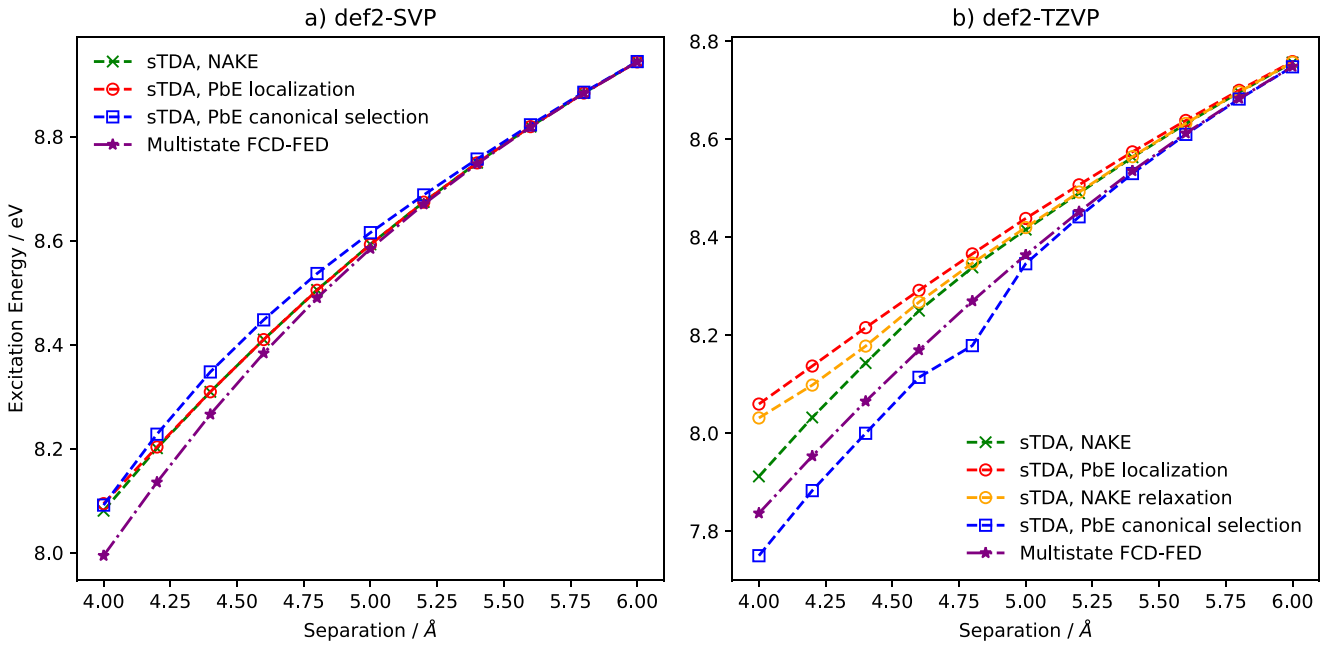

FIG. 4. FDEu-TDA and multistate FED–FCD excitation energies for the $\pi \rightarrow \pi^*$ transition from C_2F_4 to C_2H_4 in eV for varying displacements of $C_2F_4 \leftrightarrow C_2H_4$ for the (a) def2-SVP and (b) def2-TZVP basis set; "localization" uses the additional virtual orbital localization proposed in Sec. II C, "canonical" uses the partitioning of the canonical virtual orbital space proposed in Ref. 19, and "relaxation" uses an additional orthogonalization approach, as described in Sec. II C (sTDA, NAKE: CAMB3LYP/BLYP/LLP91, sTDA, PbE: CAMB3LYP/CAMB3LYP/Levelshift, and multistate FCD–FED: CAMB3LYP, 20 states).

In Fig. 4(a), the diabatic excitation energies obtained with the multistate FCD–FED method are smaller than the subsystem-based approaches. However, a fast convergence of the different methods can be observed, and the excitation energies are almost identical for inter-subsystem separations of 5.2 Å and larger. In the case of the larger def2-TZVP basis [Fig. 4(b)], more pronounced deviations in the diabatic CT excitation energies are observed, which can be explained by the larger basis-set size. For the larger basis, the orthogonality violation of the CT orbital-transition space for the approximate sTDA method is larger, which leads to deviations compared to PbE FDEu-TDA with orbital localization. This difference becomes smaller as soon as the relaxation scheme proposed in Sec. II C is used. Again, these results justify this conceptually simple ansatz to obtain CT excitation energies for approximate sTDA

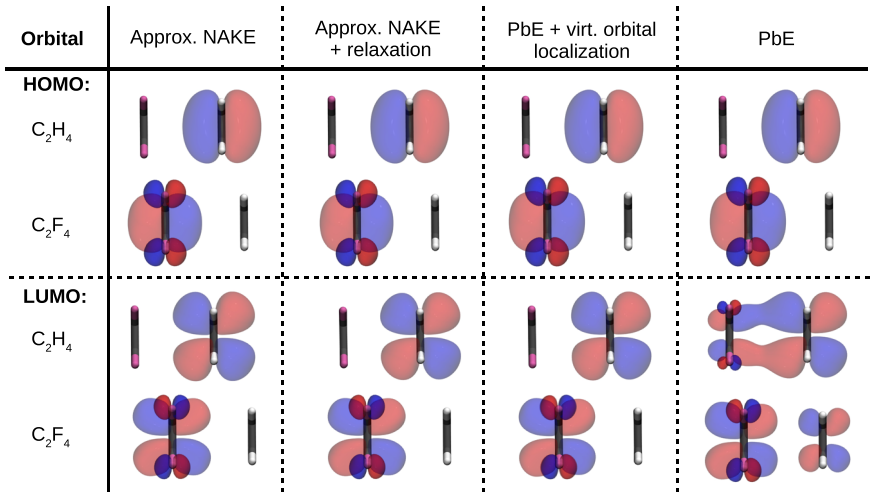

FIG. 5. Orbital isosurface (value = 0.025) plot of C_2F_4/C_2H_4 for a subsystem displacement of 4 Å obtained with projection-based embedding (PbE) and approximate non-additive kinetic embedding (Approx. NAKE); Approx. NAKE: CAMB3LYP/BLYP/LLP91; Approx. NAKE+relaxation: CAMB3LYP/BLYP/LLP91 with additional orthogonalization approach as described in Sec. II C; PbE + virt. orbital localization: CAMB3LYP/CAMB3LYP/Levelshift with additional virtual orbital localization procedure as described in Sec. II C; PbE: CAMB3LYP/CAMB3LYP/Levelshift.

calculations. In contrast, the canonical selection procedure shows a discontinuity in the excitation energy for a separation of 4.8 Å, which is caused by a different number of virtual orbitals selected for the local and CT transition orbital space compared to distances of 4.6 Å and smaller. This underlines one of the drawbacks associated with a direct selection of the canonical virtual orbitals as a diabatization procedure: These orbitals are often delocalized and change quite rapidly along a reaction coordinate, which can lead to discontinuous potential–energy curves. Note that this problem is also observed in the selection of occupied orbitals for active subsystems along reaction coordinates in ground-state PbE. There, the "even-handed" selection of orbitals is an important criterion to obtain reasonable reaction barriers.[62,63] By comparison with the multistate FED–FCD diabatization approach, excitation energies in-between those of the canonical PbE-sTDA ansatz and the other subsystem-based methods for subsystem separations between 4 Å and 5 Å can be observed. However, the excitation energies are in closer agreement with the canonical PbE-sTDA ansatz than the other diabatization procedures.

2. LE/LE electronic couplings

Next, we investigate the electronic couplings between LEs obtained with the different diabatization schemes. For this, the electronic coupling for the $\pi \rightarrow \pi^*$ excitation located on C_2F_4 and C_2H_4 for different subsystem separations is compared. The absolute electronic couplings for different subsystem displacements and basis sets are shown in Fig. 6. There, it can be seen that all methods, again, converge to the same electronic coupling at larger displacements. Furthermore, the basis set dependence of the LE/LE electronic couplings is small, and the spread in the results for the same method with the two basis sets is less than 15 meV. The deviation is increasing with smaller subsystem separations, and a fast convergence for all methods to the same coupling values can be observed. For a separation of 5 Å, the largest deviation is already below 1 kcal/mol. Interestingly, smaller couplings are obtained with the larger def2-TZVP basis for multistate FED–FCD and PbE sTDA with localization. This can be caused by a larger differential overlap of the orbitals and therefore more pronounced short-range effects. This may also explain why this trend cannot be observed for the approximate sTDA couplings. In this case, the usage of a non-additive kinetic-energy functional minimizes the overlap between densities and therefore also orbitals between subsystems.[64] However, also a reduction in the oscillator strengths for the $\pi \rightarrow \pi^*$ excitations, especially in the PbE sTDA calculations for the larger def2-TZVP basis, contributes to the observed trend. The canonical virtual-orbital selection again shows discontinuities in the electronic-coupling curves. However, the couplings are in good agreement with the other approaches shown.

Note that the comparison of the methods used here includes two reference methods that are exact in the sense that they reproduce the supermolecular adiabatic excitation energies. This holds both for PbE in combination with sTDDFT/sTDA in the full orbital transition space and for the multistate FED–FCD diabatization procedure. It should be emphasized that this does not mean that the diabatic excitation energies and couplings are identical, due to the non-uniqueness of the diabatization. Additional double logarithmic plots and analysis of the distant-dependent behavior of the LE/LE electronic couplings can be found in Sec. S2 of the supplementary material.

3. LE/CT electronic couplings

In a last step, the electronic coupling between the local $\pi \rightarrow \pi^*$ excitation on C_2H_4 (a) and C_2F_4 (b) with the CT $\pi \rightarrow \pi^*$ excitation from C_2F_4 to C_2H_4 for the different diabatization schemes are compared. First, only sTDA electronic couplings obtained with PbE are compared to the multistate FED–FCD scheme. The electronic couplings for the def2-SVP and the def2-TZVP basis set are displayed in Fig. 7, again for varying inter-subsystem separations. For the hole-transfer coupling in Fig. 7(a), all curves show an exponential decay with increasing separation.[32] A more detailed analysis of this aspect

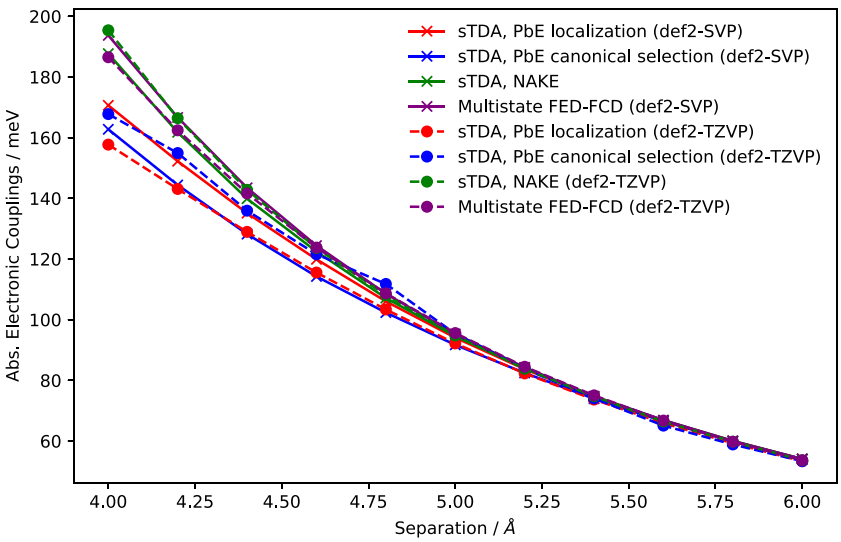

FIG. 6. LE/LE electronic couplings obtained from FDEc-TDA calculations for the $\pi \rightarrow \pi^*$ excitations located on C_2F_4 and C_2H_4 for varying separations between the subsystems; "localization" uses the additional virtual orbital localization proposed in Sec. II C, "canonical" uses the partitioning of the canonical virtual orbital space proposed in Ref. 19, and "relaxation" uses an additional orthogonalization approach, as described in Sec. II C (sTDA, NAKE: CAMB3LYP/BLYP/LLP91, sTDA, PbE: CAMB3LYP/CAMB3LYP/Levelshift, and multistate FCD–FED: CAMB3LYP, 20 states).

can be found in Sec. S2 of the supplementary material. However, the spread in the electronic coupling is significantly larger than in the case of the LE/LE electronic couplings (Fig. 6) for both the basis set dependence and the different methods. Interestingly, almost identical results are found for the multistate FED–FCD diabatization approach and the PbE-sTDA calculations with orbital localization for both basis sets in the entire displacement range. The largest deviation is less than 3 meV (4.0 Å separation, def2-SVP basis set). In contrast to that, hole-transfer couplings obtained with the canonical sTDA approach are significantly larger. Nevertheless, the qualitative behavior and basis set dependence are similar, with a slower decay of the electronic couplings for the larger def2-TZVP basis. In Fig. 7(b), the electron-transfer couplings are shown. Here, a large spread in the electronic couplings between the methods and basis set used can be observed. Especially, the couplings obtained with the canonical selection of the virtual orbitals differ significantly from the other methods and show discontinuities in the case of the larger def2-TZVP basis set. It becomes obvious that a selection of canonical orbitals is unsuited for the description of electron-transfer couplings.

In order to compare the electron-transfer couplings for the multistate FED–FCD and the localized PbE sTDA scheme more clearly, these were separated from the canonical selection and displayed in Fig. 8. For the def2-SVP basis set [Fig. 8(a)], similar electronic couplings for the multistate FED–FCD and the localized PbE sTDA scheme are obtained at least for separations larger than 4.8 Å. However, the deviations become larger for short separations, and for 4 Å, the difference is 56 meV. Enlarging the basis set [Fig. 8(b)] leads to more pronounced deviations between the two methods, and no convergence to a common value can be observed within the displacement range shown. A possible explanation for the difference between the two methods for the description of electron-transfer coupling compared to hole-transfer coupling can be found by analyzing the major coupling contribution in the subsystem case. The contributions to the electronic coupling for PbE sTDA calculations with localized orbitals are displayed in Table II. There, the main contribution to the electron-transfer is caused by the Lagrange multiplier $\delta_{ij}^{IJ} F_{ab}^{IJ}$ in the inter-subsystem Fock-matrix block. In the case of a hole-transfer coupling, the major contributions are caused by the Lagrange multiplier $\delta_{ab}^{IJ} F_{ij}^{IJ}$. Both contributions are directly related to the orbital localization procedure and therefore to the diabatization procedure employed. Due to the overall more delocalized shape of virtual orbitals, the resulting virtual–virtual block in the Fock-matrix depends more strongly on the unitary transformation. This could be an explanation for the difference between the multistate FED–FCD diabatization and the PbE sTDA method with localized orbitals. More details concerning these discrepancies can be found in Sec. S1 of the supplementary material.

In the next step, hole- and electron-transfer couplings from the approximate sTDA procedure are compared to PbE-sTDA couplings with orbital localization. The comparison is displayed in Fig. 9. For the electronic couplings from approximate sTDA in def2-SVP basis without an additional correction (Fig. 9; gray dashed line), it becomes apparent that the electronic couplings are heavily underestimated. For PbE-sTDA with orbital localization, it was already observed that the main contribution to the electronic

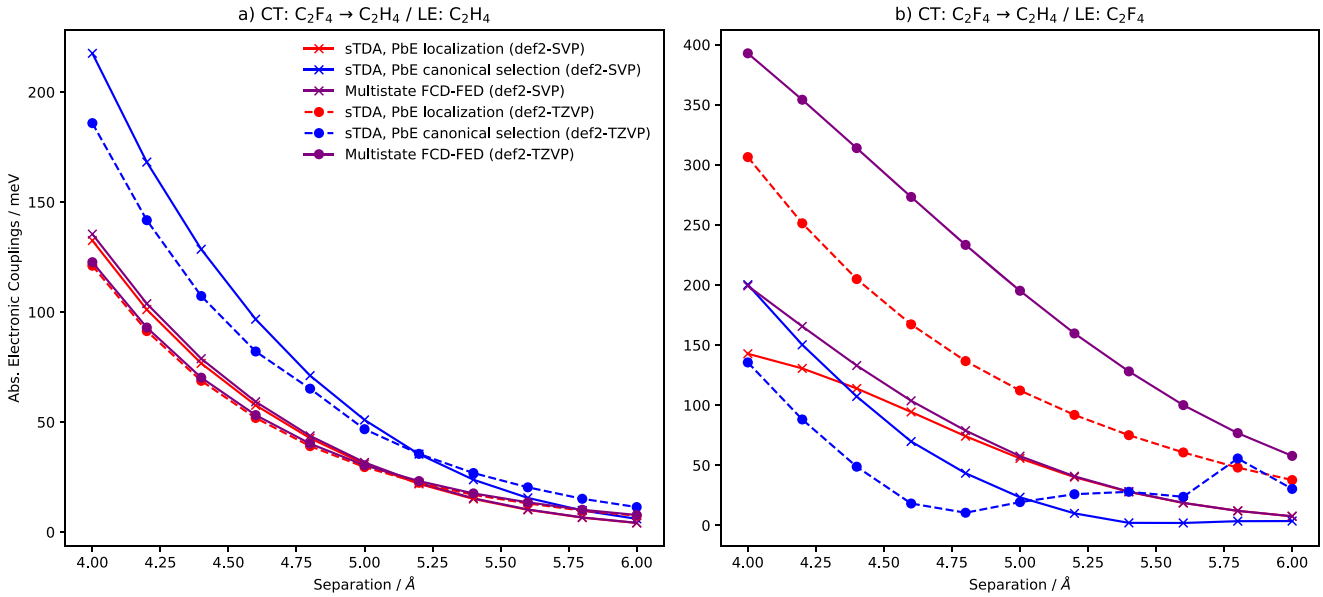

FIG. 7. LE/CT electronic couplings obtained from FDEc-TDA calculations for (a) the $\pi \rightarrow \pi^*$ excitations located on C_2H_4 and $\pi \rightarrow \pi^*$ from C_2F_4 to C_2H_4 and (b) the $\pi \rightarrow \pi^*$ excitations located on C_2F_4 and $\pi \rightarrow \pi^*$ from C_2F_4 to C_2H_4 for varying separations between the subsystems; "localization" uses the additional virtual orbital localization proposed in Sec. II C and "canonical" uses the partitioning of the canonical virtual orbital space proposed in Ref. 19 (sTDA, PbE: CAMB3LYP/CAMB3LYP/Levelshift and multistate FCD–FED: CAMB3LYP, 20 states).

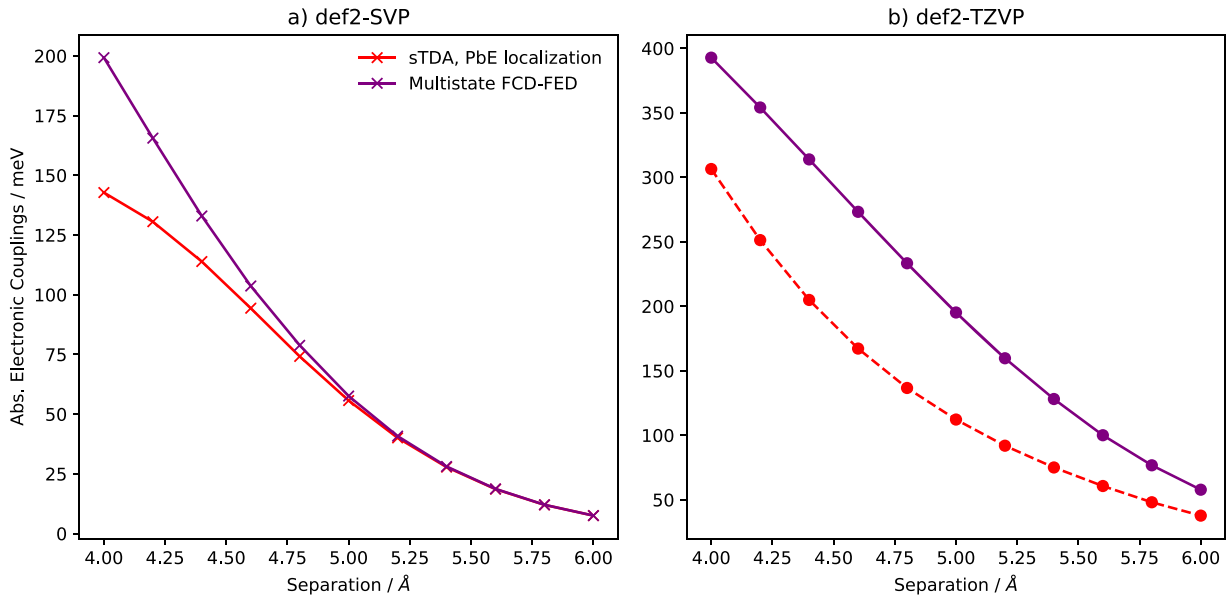

FIG. 8. Electron transfer couplings ($\pi \rightarrow \pi^*$ excitation located on C_2F_4 and $\pi \rightarrow \pi^*$ from C_2F_4 to C_2H_4) for varying separations between the subsystems and basis sets, (a) def2SVP and (b) def2-TZVP; "localization" uses the additional virtual orbital localization proposed in Sec. II C (sTDA, PbE: CAMB3LYP/CAMB3LYP/Levelshift and multistate FCD–FED: CAMB3LYP, 20 states).

coupling is caused by inter-subsystem occupied–occupied/virtual–virtual Fock-matrix block, which represents off-diagonal Lagrange multipliers arising from the orbital localization procedure.[19] By interpreting the diabatization in the approximate sTDA procedure also as a (non-orthogonal) localization procedure, these off-diagonal Lagrange multipliers are missing in this approach. We therefore corrected our model by these missing Lagrange multipliers ($S_{ij}F_{ab}$ for hole-transfer and $S_{ab}F_{ij}$ for electron-transfer). However, it has to be noted that these corrections represent pragmatic corrections with empirical flavor because the orbitals of different subsystems in sDFT with the approximate NAKE functional are not required to be orthogonal.[48] We therefore scale the different Lagrange multipliers and compare the couplings with those obtained from PbE-sTDA with orbital localization. In addition, the largest orbital overlap is always subtracted from the scaling factor in order to correct for non-orthogonality. This means that in the case of an electron-transfer, the correction is scaled with $[a_{\text{scaling}} - \max(S_{ij})]S_{ij}F_{ab}$. The curves for different scaling factors are shown in Fig. 9. In Fig. 9(a), reasonable agreement for the def2-SVP and def2-TZVP basis set compared to PbE-sTDA can be observed for a scaling factor of $a_{\text{scaling}} = 0.25$, while the electronic couplings obtained from $a_{\text{scaling}} = 1.0$ are overestimated. In the case of hole-transfer, a reasonable agreement with PbE-sTDA with the def2-SVP for a scaling factor of $a_{\text{scaling}} = 1.0$ is achieved. However, the situation changes for the larger def2-TZVP basis. Here also, a qualitatively wrong distance dependence of the electronic coupling can be observed.

It can be seen that the proposed approximate sTDA approach for the calculation for hole-and electron-transfer coupling is highly dependent on the basis set and the empirically scaled factor for the off-diagonal Lagrange multiplier, which effectively makes this method unsuitable as a general tool. However, we

TABLE II. LE/CT electronic coupling contributions obtained from PbE-sTDA calculations for the $\pi \rightarrow \pi^*$ excitations located on C_2H_4/C_2F_4 and $\pi \rightarrow \pi^*$ from C_2F_4 to C_2H_4 (hole-transfer, electron-transfer) for an inter-subsystem separation of 5.0 Å.

	Abs. Electronic Coupling/meV			
	$CT(C_2F_4 \rightarrow C_2H_4)/LE(C_2H_4)$		$CT(C_2F_4 \rightarrow C_2H_4)/LE(C_2F_4)$	
Coupling contribution	def2-SVP	def2-TZVP	def2-SVP	def2-TZVP
Full [Eq. (12)]	31	30	56	160
Neglection of Eq. (22)	3	4	1	5
Coulomb only	4	1	1	1

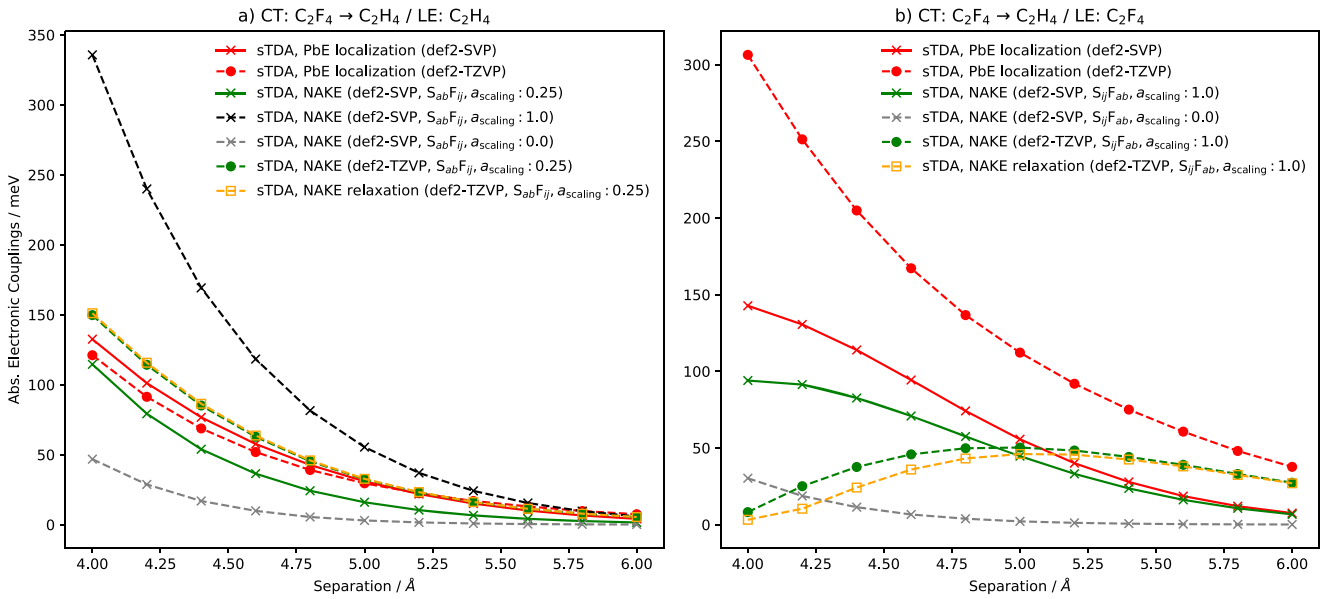

FIG. 9. LE/CT electronic couplings obtained from FDEc-TDA calculations for (a) the $\pi \rightarrow \pi^*$ excitations located on C_2H_4 and $\pi \rightarrow \pi^*$ from C_2F_4 to C_2H_4 and (b) the $\pi \rightarrow \pi^*$ excitations located on C_2F_4 and $\pi \rightarrow \pi^*$ from C_2F_4 to C_2H_4 for varying separations between the subsystems; "localization" uses the additional virtual-orbital localization proposed in Sec. II C, "canonical" uses the partitioning of the canonical virtual orbital space proposed in Ref. 19, and "relaxation" uses an additional orthogonalization approach, as described in Sec. II C (sTDA, NAKE: CAMB3LYP/BLYP/LLP91 and sTDA, PbE: CAMB3LYP/CAMB3LYP/Levelshift).

want to emphasize that this approach seems suitable for the calculation of charge-transfer excitation energies as demonstrated earlier.

B. Adenine–thymine

In a next step, the adenine–thymine (AT) base pair is used as a biologically relevant test system for the evaluation of electronic couplings based on sTDA and the multistate FED–FCD scheme. This example is chosen due to the rich and complex photophysics of DNA (cf. Refs. 65–69) and therefore represents a realistic model system to use different diabatization approaches to obtain electronic couplings. The structure used in the following was taken from Ref. 70 and is displayed in Fig. 10.

In Ref. 70, the electronic couplings associated with the two lowest diabatic excitations located on adenine and thymine and the lowest CT excitation from adenine to thymine were investigated by means of MS-CASPT2. In order to compare these couplings to couplings obtained from TDDFT in the TDA, benchmark calculations of the supersystem were performed employing the CAMB3LYP and LCBLYP[71] (μ = 0.33 bohr^{-1}) exchange–correlation functionals. Excitation energies and oscillator strength (length gauge is chosen throughout this study) are further compared with respect to CC2 and ADC(2), employing the def2-TZVP basis set and the RI approximation. The CC2 and ADC(2) calculations were performed with TURBOMOLE V7.4.1.[72,73] The results are shown in Table III. For the excitation energies obtained in Ref. 70, a (10, 10) active space was chosen so that the MS-CASPT2 results correspond to transitions predominantly of $\pi \rightarrow \pi^*$ type. The resulting $\pi \rightarrow \pi^*$ transitions are compared in the following. The state assignment in Table III is based on the predominant contributions. However, especially, the L_b state is accompanied with additional orbital transitions contributing to the excitation.

For the adenine–thymine base pair, the CC2 excitation energies are blue shifted, compared to the ADC(2) results by about 0.08 eV. However, similar oscillator strengths are obtained for both approaches. By comparison of the ADC(2) and CC2 excitation

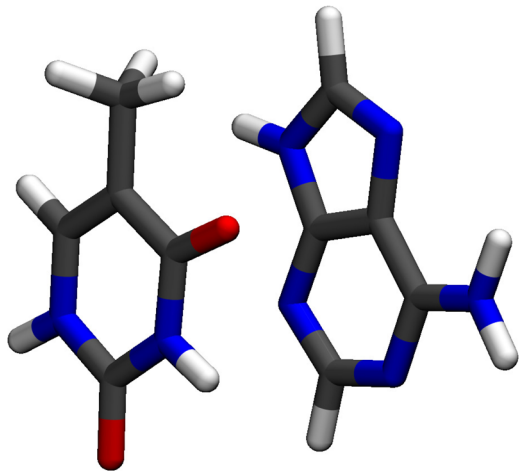

FIG. 10. Adenine–thymine DNA base pair taken from Ref. 70.

TABLE III. Adiabatic excitation energies and oscillator strength (length gauge) for the adenine–thymine base pair, as displayed in Fig. 10. The def2-TZVP basis set is used, and TDDFT calculations were performed employing the TDA.

	Excitation Energy (oscillator strength)/eV (au)				
	MS-CASPT2	CC2	ADC(2)	CAMB3LYP	LCBLYP
$A(L_a)$	5.58(0.272)[a]	5.35(0.248)	5.26(0.238)	5.60(0.182)[b]	5.67(0.300)
$A(L_b)$		5.25(0.009)	5.19(0.026)	5.62(0.111)[b]	5.51(0.004)
$T(\pi\pi^*)$	4.95(0.304)[a]	5.14(0.131)	5.06(0.147)	5.36(0.134)	5.33(0.157)
$A \rightarrow T(\pi\pi^*)$	5.30(0.160)[a]	5.59(0.001)	5.52(0.002)	5.18(0.025)	5.90(0.004)

[a]Taken from Ref. 70.
[b]A mixing of L_a and L_b can be observed the assignment is based on the predominant contribution.

energies to the MS-CASPT2 results of Ref. 70, a difficulty arises in the characterization of the adiabatic excitation mostly located on adenine. While no assignment for this state was given in Ref. 70, the state was characterized as L_a in Ref. 69. Therefore, this characterization is adopted in Table III. In the following, the MS-CASPT2 excitation energies and oscillator strengths are compared to the results obtained with ADC(2) and CC2. The excitation energy of the L_a state is larger by 0.23 eV compared to CC2 and by 0.32 eV compared to ADC(2). Nevertheless, a similar oscillator strength can be observed. In the case of the $\pi \rightarrow \pi^*$ excitation mostly located on the thymine, better agreement in the excitation energy compared to CC2 and ADC(2) is obtained, while the oscillator strength differs significantly. Comparing the lowest CT state from adenine to thymine, a different ordering compared to CC2 and ADC(2) can be observed. While the CT state lies energetically between the local excitations on A and T in the case of the MS-CASPT2 calculations, the CT excitation is shifted to higher energies in the case of CC2 and ADC(2) and lies approximately 0.3 eV above the L_a excitation. In Ref. 70, the low-lying CT state was already discussed and the difference to previous wavefunction-based calculations[74] on the adenine–thymine dimer was mentioned. In Ref. 74, the CT state was found about 0.4 eV above the local $\pi \rightarrow \pi^*$ excited state on adenine and thymine in the case of EOM-CCSD(T) and about 0.3 eV in the case of ADC(2). In Ref. 70, it was argued that this deviation arises from differences in the geometry, especially the stacking distance, of the base pair. The results shown here for ADC(2) and CC2 confirm the energetical separation of local and CT states observed in Ref. 74 although the structure of Ref. 70 is used. Here, the CT state is about 0.26 eV and 0.24 eV, respectively, higher in energy than the local excited states. Furthermore, a significant difference in the oscillator strength for the CT transition can be observed. This raises the question if a larger active space than the one employed in the MS-CASPT2 calculations in Ref. 70 would lead to results closer to the other methods.

In a next step, the CC2 and ADC(2) excitation energies and oscillator strength are compared to TDDFT within the TDA for the CAMB3LYP and LCBLYP(μ = 0.33 $bohr^{-1}$) exchange–correlation functional. While the results for LCBLYP compared to CC2 and ADC(2) show the same energetical order and similar oscillator strengths, a blue shift in the absolute excitation energies can be observed. However, the overall good agreement in the energetic order and the agreement in the oscillator strength indicates the capability of TDA with the LCBLYP exchange–correlation functional to give a consistent picture of the vertical excitation energies compared to CC2 and ADC(2). In contrast, results obtained with the CAMB3LYP functional lead to a significant mixing of the L_a and L_b states and an energetically low-lying CT excitation.

Electronic couplings and diabatic excitation energies for this particular system were obtained in Ref. 70, employing a three-state model. Here, we compare these results to those obtained with the diabatization procedures used in Sec. IV A. The results are listed in Table IV. In Ref. 70, a mixing of the three states was observed, which required the usage of a three-state model in order to disentangle these states in the diabatic representation and to extract electronic couplings. For the TDA calculations performed here, the def2-SVP and def2-TZVP basis sets in combination with the CAMB3LYP and LCBLYP exchange–corelation functional were used. As analyzed in Sec. IV A, the most consistent couplings were obtained using PbE sTDA in combination with an additional virtual orbital localization procedure. This procedure is therefore employed in the following. However, it is computationally the most demanding procedure of the subsystem-based methods compared in Sec. IV A. We therefore introduce an approximation in the coupling step. For this, the inter-subsystem exact exchange is not evaluated, which should introduce a negligible error due to the fact that electron- and hole-transfer couplings are predominantly captured by off-diagonal Lagrange-multipliers caused by the orbital localization of the occupied and virtual orbital space (Table II). This approximation is achieved by replacing the inter-subsystem exchange–correlation functional (CAMB3LYP/LCBLYP) with BLYP and is tested against PbE sTDA calculations without any additional approximations.

We start by comparing the diabatic excitation energies based on the multistate FED–FCD diabatization procedure and sTDA. For all diabatic excitation energies, an expected decrease in excitation energies with an increase in the basis set can be observed. Almost no exchange–correlation functional dependence for the diabatic $\pi \rightarrow \pi^*$ excitation energies on thymine within a given basis set and diabatization procedure is observed. However, the excitation energies obtained with the subsystem-based approach are constantly shifted by about +0.12 eV relative to the multistate FED–FCD scheme. Similar deviations in the diabatic excitation energies can also be observed for the other local and CT diabatic excitation energies.

TABLE IV. Electronic couplings and diabatic excitation energies for the adenine–thymine base pair, as displayed in Fig. 10.

	Electronic coupling/meV					Excitation energy/eV			
Method	$\lvert V_{L_a,T}\rvert$	$\lvert V_{L_b,T}\rvert$	$\lvert V_{CT,L_a}\rvert$	$\lvert V_{CT,L_b}\rvert$	$\lvert V_{CT,T}\rvert$	ϵ_{L_a}(A)	ϵ_{L_b}(A)	ϵ(T)	ϵ_{CT}(A → T)
MS-CASPT2 (ANO-S) 3 states (from Ref. 70)	96.3	...	137	...	99.9	5.506	...	5.018	5.315
CAMB3LYP/CAMB3LYP/Level. (def2-SVP)	7	7	29	108	51	5.91	5.73	5.68	5.49
CAMB3LYP/BLYP/Level. (def2-SVP)	7	7	25	105	46	5.91	5.73	5.68	5.49
CAMB3LYP/CAMB3LYP/Level. (def2-TZVP)	1	6	5	99	54	5.75	5.69	5.55	5.44
CAMB3LYP/BLYP/Level. (def2-TZVP)	1	6	3	102	48	5.75	5.69	5.55	5.44
Multistate FCD/FED (20 States,def2-SVP)	11	6	38	121	49	5.81	5.65	5.55	5.40
Multistate FCD/FED (20 States,def2-TZVP)	5	5	18	132	52	5.62	5.56	5.35	5.28
LCBLYP/LCBLYP/Level. (def2-SVP)	8	5	10	113	61	5.96	5.73	5.68	6.16
LCBLYP/BLYP/Level. (def2-SVP)	8	5	6	117	55	5.96	5.73	5.68	6.16
LCBLYP/LCBLYP/Level. (def2-TZVP)	2	5	34	99	65	5.81	5.68	5.55	6.10
LCBLYP/BLYP/Level. (def2-TZVP)	2	5	32	103	59	5.81	5.68	5.55	6.10
Multistate FCD/FED (20 States,def2-SVP)	11	5	12	130	60	5.87	5.65	5.56	6.03
Multistate FCD/FED (20 states, def2-TZVP)	3	3	38	134	62	5.68	5.56	5.35	5.91

Interestingly, a clear separation of L_a and L_b states in the diabatic basis for both functionals can be observed, while the supermolecular TDA calculation with the CAMB3LYP exchange–correlation functional leads to a mixing of these states. Overall, only a small dependence of the local diabatic excitation energies on the functional employed is found. By contrast, a larger difference for the CT excitation energies is obtained. Here, the results for the long-range corrected functional LCBLYP are shifted to higher energies. We now move on to the comparison of electronic couplings obtained with the sTDA approach in combination with the localization procedure. It can be seen that the approximation introduced by neglecting exact exchange in the coupling step is justified due to the small deviations caused by this approximation (a maximum deviation of 9 meV). For the local excitations, only small electronic coupling values for all procedures are obtained with a maximum value of 11 meV.

This could indicate that the coupling between the L_a and L_b located on adenine and the lowest $\pi \rightarrow \pi^*$ on thymine plays only a small role in the photophysics of this adenine–thymine stack. In addition, the electronic couplings are even further lowered by an increase in the basis set. The situation changes for the LE/CT couplings. Here, electronic couplings of about 50 meV in the case of thymine/adenine → thymine are obtained for the CAMB3LYP functional and about 60 meV for the LCBLYP functional. Similar values are obtained when changing the basis set or the diabatization procedure. This is in line with the findings in Sec. IV A (Sec. IV A), where it was already observed that hole-transfer couplings are less sensitive to the diabatization procedure employed. This situation changes for electron-transfer couplings. These are dominated by the virtual–virtual off-diagonal Lagrange multipliers in the Fock-matrix and are therefore more sensitive to the basis and the diabatization procedure. This can also be observed here. While the electronic coupling of the L_b transition with the adenine → thymine CT transition is mostly independent of the basis set, the couplings differ by about 20 meV between the methods. However, the influence of the exchange–correlation functional is relatively small. This changes for the L_a state, where the couplings decrease significantly for the CAMB3LYP functional with the larger def2-TZVP basis compared to def2-SVP, but the coupling increases for the LCBLYP functional. However, the couplings for the different diabatization procedures are again similar. Additional electronic couplings for the stacked DNA base pair for different relative separations are depicted in Sec. S3 of the supplementary material for the LCBLYP exchange–correlation functional.

Finally, we compare the electronic couplings based on the multistate FED–FCD procedure and sTDA calculations to the electronic couplings calculated in Ref. 70. As already mentioned in the analysis of supermolecular excitation energies earlier, no characterization of the lowest singlet excitation located on adenine was made in Ref. 70, and the state assignment used here was based on Ref. 69. Therefore, the same assignment for the diabatic state located on adenine is used here, and the resulting couplings are shown in Table IV. By comparison of the electronic couplings for the local excitations, a large discrepancy can be observed. While the electronic couplings from sTDA and TDA are almost negligible, a coupling of 96 meV is obtained from the MS-CASPT2 calculations. Similar differences can also be observed for the hole-transfer coupling from adenine to thymine, where the coupling is about twice as large. The differences are most probably due to the different character of the lowest–energy transitions of the dimer. A final assessment of the TDA/sTDA couplings obtained here through comparison to the MS-CASPT2 data from Ref. 70 thus remains elusive. The comparison of our TDA/sTDA results to ADC(2) and CC2 results and that to the EOM-CCSD(T) results from Ref. 74 show that these methods all seem to agree as far as the qualitative character of these states is concerned.

V. CONCLUSIONS

In summary, this paper has shown that subsystem-TDDFT within the TDA is not only capable of describing LE/LE

electronic couplings but can also properly incorporate CT excitations (excitons) in the coupling procedure. For this, different diabatization procedures within the sTDDFT framework have been proposed. For sDFT making use of NAKE functionals, a pragmatically motivated approach has been used, which combines occupied and virtual orbitals of different subsystems, opening the way to include CT excitations in typical approximate sTDDFT calculation for the first time, while diabatization of the local excitations is still achieved via basis set restriction. For sDFT and sTDDFT in the context of projection-based embedding, two diabatization procedures have been presented. One relies on the selection of canonical virtual orbitals as already described in Ref. 19, and the other performs an additional orbital localization procedure of the virtual orbital space to separate local- and CT excitations.[42] By comparison of these three diabatization approaches, it has been found that approximate sTDDFT is especially suited for the description of LE/LE electronic couplings with a relatively low computational cost. Furthermore, a description of diabatic CT excitations is possible with this variant, but the description of LE/CT couplings is error prone and not recommended. In order to describe LE/CT couplings, the additional virtual orbital localization procedure for PbE-sTDDFT has shown to be useful and reliable to obtain smooth diabatic potential energy curves and reasonable electronic couplings. Furthermore, it was found that the neglection of the exact exchange contribution in the coupling procedure only leads to small errors, while savings in the computational time can be obtained.

Besides proposing these different diabatization schemes, an in-depth comparison with a recently proposed multistate FED–FCD ansatz[25] has been performed. It was found that both approaches, although different in their general strategy, lead to similar electronic couplings in the case of local and hole-transfer couplings. In addition, a reasonable agreement can be found for electron-transfer couplings. Especially for strongly interacting subsystems, however, differences were observed. These could be traced back to off-diagonal Lagrange multipliers in the virtual–virtual block of the Fock matrix. They are therefore more sensitive to the diabatization procedure than hole-transfer couplings, which depend on the occupied–occupied block of the Fock matrix. Furthermore, the approaches were used to describe electronic couplings for a adenine–thymine DNA base pair to demonstrate their applicability in biologically relevant systems. Electronic couplings for the $\pi \rightarrow \pi^*$ diabatic local- and CT excitations were calculated. Differences occurring for this example in comparison to earlier work based on MS-CASPT2[70] were analyzed in detail based on supermolecular TDA, CC2, and ADC(2) calculations as well as on previous EOM-CCSD(T) results.[74] All these aforementioned approaches lead to a similar energetic order and character of the excitations (using an appropriate exchange–correlation functional in the case of DFT-based approaches), although a differently stacked structure was used in Ref. 74 for the EOM-CCSD(T) calculations. However, the MS-CASPT2 results in Ref. 70 show differences in oscillator strengths and energetic order, which probably translate into the observed differences for the electronic couplings and diabatic excitation energies. One possible reason for this mismatch could be the specific choice made for the active space in Ref. 70. A direct comparison of the electronic couplings shown here and calculated in Ref. 70 remains therefore elusive. However, subsystem-TDA and the multistate FED–FCD procedure again lead to a good agreement for the calculated electronic couplings.

Overall, this work extends the range of applicability of sTDDFT as a useful and versatile tool for the calculation of electronic couplings. While approximate sTDDFT is especially suited and computationally appealing for the description of LE/LE couplings, PbE-sTDDFT with an additional virtual orbital localization is capable of describing all couplings shown in Fig. 1 and therefore represents a complete toolbox. Furthermore, a good overall agreement to another widely used diabatization procedure, namely, the multistate FED–FCD approach,[25,75–77] has been found, which underlines the usefulness of both approaches.

SUPPLEMENTARY MATERIAL

See the supplementary material for a comparison of the natural-transition orbitals (NTOs) for the multistate FED–FCD procedure and sTDA with virtual orbital localization for tetrafluoroethylene–ethylene for a separation of 4 Å, logarithmic plots and slopes for the distance-dependence of the electronic couplings for tetrafluoroethylene–ethylene, the distance-dependence of the electronic couplings for the adenine–thymine base pair, and comparison of multistate FED–FCD procedure and sTDA with virtual orbital localization in both cases.

DEDICATION

Dedicated to Professor Evert Jan Baerends on the occasion of his 75th birthday.

ACKNOWLEDGMENTS

L.C. and B.M. acknowledge funding by the European Research Council under the Grant No. ERC-AdG-786714 (LIFETimeS).

DATA AVAILABILITY

The data that support the findings of this study are available within the article and/or from the corresponding author upon reasonable request.

REFERENCES

[1] C. König and J. Neugebauer, ChemPhysChem **13**, 386 (2012).
[2] N. S. Sariciftci, L. Smilowitz, A. J. Heeger, and F. Wudl, Science **258**, 1474 (1992).
[3] R. E. Blankenship, *Molecular Mechanisms of Photosynthesis* (Blackwell Science, Oxford, 2002).
[4] M. R. Wasielewski, Chem. Rev. **92**, 435 (1992).
[5] J. Neugebauer, ChemPhysChem **10**, 3148 (2009).
[6] T. A. Wesolowski and A. Warshel, J. Phys. Chem. **97**, 8050 (1993).
[7] T. A. Wesolowski and J. Weber, Chem. Phys. Lett. **248**, 71 (1996).
[8] G. Senatore and K. R. Subbaswamy, Phys. Rev. B **34**, 5754 (1986).
[9] M. D. Johnson, K. R. Subbaswamy, and G. Senatore, Phys. Rev. B **36**, 9202 (1987).
[10] P. Cortona, Phys. Rev. B **44**, 8454 (1991).
[11] T. A. Wesolowski, J. Am. Chem. Soc. **126**, 11444 (2004).
[12] M. E. Casida and T. A. Wesołowski, Int. J. Quantum Chem. **96**, 577 (2004).
[13] J. Neugebauer, J. Chem. Phys. **126**, 134116 (2007).

[14]T. Förster, Ann. Phys. **437**, 55 (1948).
[15]R. A. Marcus and N. Sutin, Biochim. Biophys. Acta **811**, 265 (1985).
[16]J. Neugebauer, J. Phys. Chem. B **112**, 2207 (2008).
[17]C. König, N. Schlüter, and J. Neugebauer, J. Chem. Phys. **138**, 034104 (2013).
[18]C. König and J. Neugebauer, J. Chem. Theory Comput. **9**, 1808 (2013).
[19]J. Tölle, M. Böckers, N. Niemeyer, and J. Neugebauer, J. Chem. Phys. **151**, 174109 (2019).
[20]F. R. Manby, M. Stella, J. D. Goodpaster, and T. F. Miller III, J. Chem. Theory Comput. **8**, 2564 (2012).
[21]J. Tölle, M. Böckers, and J. Neugebauer, J. Chem. Phys. **150**, 181101 (2019).
[22]S. Difley and T. Van Voorhis, J. Chem. Theory Comput. **7**, 594 (2011).
[23]W. Liu, B. Lunkenheimer, V. Settels, B. Engels, R. F. Fink, and A. Köhn, J. Chem. Phys. **143**, 084106 (2015).
[24]X. Li, R. M. Parrish, F. Liu, S. I. L. Kokkila Schumacher, and T. J. Martínez, J. Chem. Theory Comput. **13**, 3493 (2017).
[25]M. Nottoli, S. Jurinovich, L. Cupellini, A. T. Gardiner, R. Cogdell, and B. Mennucci, Photosynth. Res. **137**, 215 (2018).
[26]T. Van Voorhis, T. Kowalczyk, B. Kaduk, L.-P. Wang, C.-L. Cheng, and Q. Wu, Annu. Rev. Phys. Chem. **61**, 149 (2010).
[27]T. Pacher, L. Cederbaum, and H. Köppel, Adv. Chem. Phys. **84**, 293 (1993).
[28]M. Pavanello and J. Neugebauer, J. Chem. Phys. **135**, 134113 (2011).
[29]J. Neugebauer, C. Curutchet, A. Muñoz-Losa, and B. Mennucci, J. Chem. Theory Comput. **6**, 1843 (2010).
[30]C. Curutchet, A. Muñoz-Losa, S. Monti, J. Kongsted, G. D. Scholes, and B. Mennucci, J. Chem. Theory Comput. **5**, 1838 (2009).
[31]A. A. Voityuk and N. Rösch, J. Chem. Phys. **117**, 5607 (2002).
[32]C.-H. Yang and C.-P. Hsu, J. Chem. Phys. **139**, 154104 (2013).
[33]A. Goez and J. Neugebauer, "Embedding methods in quantum chemistry," in *Frontiers of Quantum Chemistry*, edited by M. Wojcik, H. Nakatsuji, B. Kirtman, and Y. Ozaki (Springer, Tokyo, 2017), pp. 139–179.
[34]F. Libisch, C. Huang, and E. A. Carter, Acc. Chem. Res. **47**, 2768 (2014).
[35]J. Nafziger and A. Wasserman, J. Phys. Chem. A **118**, 7623 (2014).
[36]C. R. Jacob and J. Neugebauer, Wiley Interdiscip. Rev.: Comput. Mol. Sci. **4**, 325 (2014).
[37]T. A. Wesolowski, S. Shedge, and X. Zhou, Chem. Rev. **115**, 5891 (2015).
[38]A. Krishtal, D. Ceresoli, and M. Pavanello, J. Chem. Phys. **142**, 154116 (2015).
[39]M. Bensberg and J. Neugebauer, J. Chem. Phys. **150**, 184104 (2019).
[40]C. R. Jacob, S. M. Beyhan, and L. Visscher, J. Chem. Phys. **126**, 234116 (2007).
[41]M. Böckers and J. Neugebauer, J. Chem. Phys. **149**, 074102 (2018).
[42]L. Scholz, J. Tölle, and J. Neugebauer, Int. J. Quantum Chem. **120**, e26213 (2020).
[43]D. Claudino and N. J. Mayhall, J. Chem. Theory Comput. **15**, 1053 (2019).
[44]M. Pavanello and J. Neugebauer, J. Chem. Phys. **135**, 234103 (2011).
[45]M. Pavanello, T. Van Voorhis, L. Visscher, and J. Neugebauer, J. Chem. Phys. **138**, 054101 (2013).
[46]A. Solovyeva, M. Pavanello, and J. Neugebauer, J. Chem. Phys. **140**, 164103 (2014).
[47]A. Schulz and C. R. Jacob, J. Chem. Phys. **151**, 131103 (2019).
[48]J. P. Unsleber, J. Neugebauer, and C. R. Jacob, Phys. Chem. Chem. Phys. **18**, 21001 (2016).
[49]C.-P. Hsu, Z.-Q. You, and H.-C. Chen, J. Phys. Chem. C **112**, 1204 (2008).
[50]A. Dreuw and M. Head-Gordon, Chem. Rev. **105**, 4009 (2005).
[51]J. P. Unsleber, T. Dresselhaus, K. Klahr, D. Schnieders, M. Böckers, D. Barton, and J. Neugebauer, J. Comput. Chem. **39**, 788 (2018).
[52]D. Barton, M. Bensberg, M. Böckers, T. Dresselhaus, P. Eschenbach, L. Hellmann, K. Klahr, A. Massolle, N. Niemeyer, D. Schnieders, J. Tölle, J. P. Unsleber, and J. Neugebauer 2020 Zenodo, qcserenity/serenity: Release 1.3.0. https://doi.org/10.5281/zenodo.4032651.
[53]N. Niemeyer, J. Tölle, and J. Neugebauer, J. Chem. Theory Comput. **16**, 3104 (2020).
[54]K. Eichkorn, O. Treutler, H. Öhm, M. Häser, and R. Ahlrichs, Chem. Phys. Lett. **240**, 283 (1995).
[55]F. Weigend, A. Köhn, and C. Hättig, J. Chem. Phys. **116**, 3175 (2002).
[56]T. Yanai, D. P. Tew, and N. C. Handy, Chem. Phys. Lett. **393**, 51 (2004).
[57]A. D. Becke, Phys. Rev. A **38**, 3098 (1988).
[58]C. Lee, W. Yang, and R. G. Parr, Phys. Rev. B **37**, 785 (1988).
[59]H. Lee, C. Lee, and R. G. Parr, Phys. Rev. A **44**, 768 (1991).
[60]F. Weigend and R. Ahlrichs, Phys. Chem. Chem. Phys. **7**, 3297 (2005).
[61]A. Dreuw, J. L. Weisman, and M. Head-Gordon, J. Chem. Phys. **119**, 2943 (2003).
[62]M. Welborn, F. R. Manby, and T. F. Miller III, J. Chem. Phys. **149**, 144101 (2018).
[63]M. Bensberg and J. Neugebauer, J. Chem. Phys. **150**, 214106 (2019).
[64]M. Humbert-Droz, X. Zhou, S. V. Shedge, and T. A. Wesolowski, Theor. Chem. Acc. **133**, 1405 (2014).
[65]C. Murphy, M. Arkin, Y. Jenkins, N. Ghatlia, S. Bossmann, N. Turro, and J. Barton, Science **262**, 1025 (1993).
[66]D. Markovitsi, T. Gustavsson, and F. Talbot, Photochem. Photobiol. Sci. **6**, 717 (2007).
[67]C. T. Middleton, K. de La Harpe, C. Su, Y. K. Law, C. E. Crespo-Hernández, and B. Kohler, Annu. Rev. Phys. Chem. **60**, 217 (2009).
[68]K. Siriwong and A. A. Voityuk, Wiley Interdiscip. Rev.: Comput. Mol. Sci. **2**, 780 (2012).
[69]R. Improta, F. Santoro, and L. Blancafort, Chem. Rev. **116**, 3540 (2016).
[70]L. Blancafort and A. A. Voityuk, J. Chem. Phys. **140**, 095102 (2014).
[71]H. Iikura, T. Tsuneda, T. Yanai, and K. Hirao, J. Chem. Phys. **115**, 3540 (2001).
[72]TURBOMOLE V7.1 2016, a development of University of Karlsruhe and Forschungszentrum Karlsruhe GmbH, 1989–2007, TURBOMOLE GmbH, since 2007.
[73]S. G. Balasubramani *et al.*, J. Chem. Phys. **152**, 184107 (2020).
[74]P. G. Szalay, T. Watson, A. Perera, V. Lotrich, and R. J. Bartlett, J. Phys. Chem. A **117**, 3149 (2013).
[75]L. Cupellini, S. Caprasecca, C. A. Guido, F. Müh, T. Renger, and B. Mennucci, J. Phys. Chem. Lett. **9**, 6892 (2018).
[76]F. C. Ramos, M. Nottoli, L. Cupellini, and B. Mennucci, Chem. Sci. **10**, 9650 (2019).
[77]L. Cupellini, D. Calvani, D. Jacquemin, and B. Mennucci, Nat. Commun. **11**, 662 (2020).